January 25, 1990

Final Technical Report for Grant No. N00014-86-K-0558
Research Project Sponsored by SDIO/IST and Managed by ONR

Research period from September 1, 1986 to December 31, 1989

Electron-Impact Ionization and Electron Attachment Cross Sections of Radicals Important in Transient Gaseous Discharges

Submitted by:

Long C. Lee
Department of Electrical and Computer Engineering
San Diego State University
San Diego, CA 92182

Santosh K. Srivastava
Jet Propulsion Laboratory
California Institute of Technology
Pasadena, CA 91109

Prepared for:

Office of Naval Research
800 North Quincy Street
Arlington, VA 22217-5000

Attention: Dr. Gabriel D. Roy
Code 1132P

Abstract

Electron-impact ionization and electron attachment cross sections of radicals and excited molecules were measured using an apparatus that consists of an electron beam, a molecular beam and a laser beam. The information obtained is needed for the pulse power applications in the areas of high-power gaseous discharge switches, high-energy lasers, particle beam experiments, and electromagnetic pulse systems. The basic data needed for the development of optically-controlled discharge switches were also investigated in this program. Transient current pulses induced by laser irradiation of discharge media were observed and applied for the study of electron-molecule reaction kinetics in gaseous discharges.

Table of Contents

I. Introduction

Gaseous discharges are frequently used in high-power discharge switches, high-energy laser systems, particle beam experiments, electromagnetic pulse systems, plasma etching and deposition processing of electronic materials, ion sources, and discharge lamps. Basic electron kinetics data, such as electron-impact ionization and electron attachment cross sections of molecules and radicals, are generally needed for pulse power applications, especially for the development of optically- and/or electron beam-controlled opening switches. The basic kinetics data are also needed for the modeling of chemical process in non-discharge plasma, for example, combustion media in which electrons exist. While stable molecules are extensively studied, the electron kinetics data for radicals and excited molecules are little known. This lack of basic information hinders the progress of science and applications using gas discharges. The fundamental electron kinetics data of molecules, radicals, excited molecules, and ions are being measured in the current research program under Grant No. N00014-86-K-0558.

Transient current pulses induced by laser irradiation of discharge media have been observed in our laboratory for various gas mixtures that contain trace electronegative gases in buffer gas. These transient phenomena could be used to obtain electron-molecule reaction kinetics data and eventually electron transport parameters involving in gaseous discharges. The data obtained are aimed for the development of optically-controlled high-power discharge switches.

II. Research Accomplished

The research results obtained in the current funding period are summarized below:

A. Electron-Impact Ionization of Radicals

An apparatus that consists of an excimer laser, an electron beam, a molecular beam, and a mass spectrometer has been constructed to measure the electron-impact ionization of radicals. The schematic diagram of the apparatus is shown in Fig. 1 in the paper attached as Appendix A. The radicals were produced by laser dissociation of stable molecules that were injected into a vacuum chamber through a nozzle. The radicals were than ionized by energy-resolved electron beams. The ions produced by electron-impact ionization of radicals are analyzed and detected by a mass spectrometer.

Since radicals and excited molecules are chemically active, they exist only in very short lifetimes. It is difficult to produce sufficient high concentrations of these reactive species for experiments. This difficulty makes the measurements of electron-impact excitation cross sections a challenging task. The measurements are possible by the recent advance of high-power ultraviolet excimer lasers that can produce sufficient high concentrations of radicals by photodissociation of molecules. As an example, the electron-impact ionization cross section of the CH_3 radical has been measured in this program. The CH_3 radicals were produced by excitation of CH_3OH with ArF excimer laser photons (193 nm). Similar experimental results were obtained using other CH_3 radical sources, for example, photodissociation of CH_3Cl, $(CH_3)_2O$, and $(CH_3)_2CO$. The photoabsorption cross sections of the molecules that can be used for the CH_3 radical sources are reported in a paper attached as attached as Appendix B. The cross section

for the production of CH_3^+ by electron-impact ionization of CH_3OH was measured at the Jet Propulsion Laboratory, and was used to calibrate the detection efficiency that converted the measured CH_3^+ ion signal into absolute ionization cross section of CH_3. The results have been reported in more detail in the paper attached as Appendix A.

B. Electron-Impact Ionization of Excited Molecules

Molecules in a discharge medium could be excited by electron-impact to produce excited molecules, radicals, as well as positive and/or negative ions. Excited molecules are abundant in gaseous discharges, and play important roles in determining discharge characteristics. Electron excitation cross sections of excited molecules are thus important for theoretical modeling of discharge processes.

Similar to radicals, the data for excited molecules are little known. Excited species are chemical active, and their lifetimes are short; thus, it is difficult to measure their electron-impact excitation cross sections. The flux of excimer lasers is now so intense that they can be used to produce sufficient concentrations of excited molecules for cross section measurements. As an example, the electron-impact dissociative ionization process of excited N_2^* was investigated in this research program using the apparatus constructed for the study of radicals. The N_2 molecules were excited into the $A^3\Sigma_u^+$ metastable state by ArF laser photons, and then dissociatively ionized by electron beam. The dissociation products were analyzed and detected by a mass spectrometer. The experimental results are described in more detail in a paper attached as Appendix C.

C. Electron Attachment to Molecules in Discharges

Current switching by laser irradiation of DC discharge media has been observed in our laboratory. Discharge current increases immediately after

the laser pulse, and then decreases below the DC level before recovery. The current increase is due to photoelectrons produced by laser photodetachment of negative ions. The current could increase by a factor of about 10^3, which is equal to the ratio of electron drift velocity to negative ion drift velocity. The current decrease is likely due to electron attachment to radicals and/or excited molecules produced by laser irradiation of molecules in discharges. Since current switching is useful for the development of optically-controlled discharge switches, further studies of the electron-molecule reaction kinetics in discharges are of interest.

The current increase, ΔI, is proportional to the negative ion density, n_e, photodetachment cross section, σ_d, laser power, I_ν, and electron drift velocity, v_d, namely,

$$\Delta I = C\, n_e\, \sigma_d\, I_\nu\, v_d \qquad (1)$$

where C is a constant that includes the geometry factor and detection efficiency.

The negative ion density is an important factor in determining the magnitude of current switching. However, the densities of negative ions in discharge media that contain halogen compounds are not well studied. In the present experiment, negative ions are produced by electron attachment to electronegative gases mixed in a buffer gas. The production rate of a negative ion is determined by the electron attachment rate constant and the production yield for the ion. The electron attachment rate constants have been measured in our laboratory for many electronegative molecules, even though additional molecular data are still needed. As an example, the electron attachment rate constant of BCl_3 was measured in this research program, and the results are described in a paper attached as Appendix D.

An apparatus has been constructed to study the production mechanisms and to measure the concentrations of negative ions in discharge media as shown in Fig. 1 of Appendix D. The apparatus that consists of a mass spectrometer, an excimer laser, and a differential pump station was funded by the DOD Instrumentation Program. The negative ions produced by hollow-cathode discharges of trace electronegative molecules in a buffer are extracted to the mass spectrometer through a skimmer hole. This apparatus has been tested by analyzing the negative ions produced in the discharge medium of BCl_3 in N_2. The results are described in more detail in the paper attached as Appendix D, which has been accepted for publication in the Journal of Applied Physics.

D. Laser Detachment of Negative Ions in Discharges

Techniques for measuring the negative ion concentrations and other electron transport parameters (electron and ion drift velocities, electric fields, electron energy distributions, etc.) are being pursued. This information is needed for the theoretical modeling of discharge processes and for practical applications in the design of discharge switches; however, techniques for measuring these parameters are not well developed, and they are being investigated in this program. The results are described in detail in a paper attached as Appendix E.

III. Index of Publications and Presentations

The research results obtained in this program have been published in scientific journals and presented in scientific conferences as below:

1. *"Fluorescence Yields from Photodissociative Excitation of Chloromethanes by Vacuum Ultraviolet."* L. C. Lee and M. Suto, Chem. Phys. **114**, 423 (1987).
2. *"Laser-Induced Current Switching in Gaseous Discharges,"* L. C. Lee, W. C. Wang, and D. P. Wang, presented at the meeting of "Space Structures, Power, and Power Conditioning," Proceedings of SPIE, Vol. 871, **121** (1988).
3. *"Electron Kinetics and Optical Diagnostics for Plasma-Assisted Material Processing,"* L. C. Lee, presented at the workshop on New Directions in Plasma Engineering, University of California, Berkeley, California, June 9-10, 1988.
4. *"Electron Kinetics and Spectroscopic Data of Molecules Important in Plasma Processing of Electronic Materials,"* L. C. Lee, presented at the Gordon Research Conference on Plasma Chemistry, Tilton, New Hampshire, August 15-19, 1988.
5. *"Electron-Impact Ionization and Attachment Cross Sections of Radicals and Molecules for Applications of Gaseous Discharge Switches,"* L. C. Lee, presented at the Pulse Power Workshop, University of Rochester, New York, August 15-16, 1988.
6. *"Dissociative Ionization of Laser Excited Molecules and radicals by Electron Impact,"* D. P. wang, L. C. Lee, and S. K. Srivastava, presented at the 41st Annual Gaseous Electronics conference, Minneapolis, Minnesota, October 18-21, 1988.
7. *"Electron-Impact Ionization Cross Section of CH_3 Radical,"* L. C. Lee, D. P. Wang, and S. K. Srivastava, presented at the 1988 Fall Meeting of The Texas Section, American Physical Society, Lubbock, Texas, November 4-5, 1988.
8. *"Electron-Impact Ionization of CH_3 in 10-22 eV,"* D. P. Wang, L. C. Lee, and S. K. Srivastava, Chem. Phys. Lett. **152**, 513 (1988).
9. *"Dissociative Ionization of Laser Excited N_2^* by Electron Impact,"* D. P. Wang, L. C. Lee, and S. K. Srivastava, Int. J. Mass Spectron. Ion Proc. **88**, 267 (1989).

10. *"Negative Ion Pulses Induced by Laser Irradiation of DC Discharge Media,"* L. C. Lee, J. C. Han, and M. Suto, Abstract in the Sixth International Swarm Seminar, Webb Institute, New York, August 3-5, 1989.

11. *"Negative Ion Kinetics in BCl_3 Discharges,"* Z. Lj. Petrovic, W. C. Wang, L. C. Lee, J. C. Han, and M. Suto, presented at the Sixth International Swarm Seminar, Webb Institute, New York, August 3-5, 1989.

12. *"Low Energy Electron Attachment to BCl_3,"* Z. Lj. Petrovic, W. C. Wang, M. Suto, J. C. Han, and L. C. Lee, J. Appl. Phys. in press (1990).

13. *"Fluorescence from VUV Photoexcitation of Molecules,"* Invited Talk, presented at the 1989 International Chemical Congress of Pacific Basin Societies, Honolulu, Hawaii, December 17-22, 1989.

14. *"Cross Sections for the Production of Positive Ions by Electron-Impact on Methyl Alcohol,"* E. Krishnakumar and S. K. Srivastava, to be submitted to Phys. Rev. A (1990).

15. *"Transient Signals Induced by Laser Irradiation of Negative Ions in Hollow Electrode Discharges of Cl_2 and HCl in N_2,"* J. C. Han, M. Suto, L. C. Lee, and Z. Lj. Petrovic, to be submitted to J. Appl. Phys. (1990).

IV. Index of Technical Reports

1. "Publications/Patents/Presentations/Honors" Report, submitted on October 22, 1986.
2. Annual Report for the Research Period from September 1, 1986 to December 31, 1987, submitted on February 5, 1988.
3. One Page Report submitted on August 22, 1988.
4. Annual Report for the Research Period from January 1, 1988 to September 30, 1988, submitted on October 12, 1988.
5. One Page Report submitted on July 1, 1989.
6. "End-of-the-Fiscal-Year" Letter Report, submitted on September 25, 1989.
7. "Publications/Patents/Presentations/Honors" Report, submitted on October 26, 1989.

V. Appendices

A. Electron-impact ionization of CH_3 in 10-22 eV.

B. Fluorescence yields from photodissociative excitation of chloromethanes by vacuum ultraviolet.

C. Dissociative ionization of laser excited N_2 by electron impact.

D. Low energy electron attachment to BCl_3.

E. Transient signals induced by laser irradiation of negative ions in hollow electrode discharges of Cl_2 and HCl in N_2.

Volume 152, number 6 CHEMICAL PHYSICS LETTERS 25 November 1988

ELECTRON-IMPACT IONIZATION OF CH_3 IN 10–22 eV

D.P. WANG, L.C. LEE [1]

Department of Electrical and Computer Engineering, San Diego State University, San Diego, CA 92182, USA

and

S.K. SRIVASTAVA

Jet Propulsion Laboratory, California Institute of Technology, Pasadena, CA 91109, USA

Received 8 August 1988; in final form 16 September 1988

Methyl radicals (CH_3) were produced by photodissociation of CH_3OH with ArF excimer laser photons at 193 nm. Electron-impact ionization cross sections of CH_3 were measured at electron energies from ionization threshold (9.84 eV) to 14 eV. The electron-impact ionization cross sections for dissociation of CH_3OH into various fragment ions at 100 eV are also reported in this paper.

1. Introduction

Radicals are abundant in discharge media that are mainly produced by electron-impact dissociation of stable molecules. Electron-impact ionization cross sections of radicals are the most fundamental data needed for understanding the radical chemistry in gaseous discharges. However, the data for radicals are sparse because of experimental difficulty. This paper reports the measurement of CH_3. The data are needed for modeling gaseous discharge media containing methyl compounds, which are frequently used for the CH_3 radical sources in diamond film deposition and for the study of fast gaseous discharge switches as well.

In the current experiment, the CH_3 radical was produced by photodissociation of CH_3OH by ArF excimer laser photons at 193 nm. CH_3 was then ionized by electron impact. The electron-impact ionization cross section was determined by comparing the CH_3^+ ion intensity observed from electron impact of CH_3 with that of CH_3OH.

[1] Also at the Department of Chemistry, San Diego State University, San Diego, CA 92182, USA

2. Experimental

2.1. Apparatus

The experimental apparatus is shown in fig. 1. The apparatus consists of an electron beam, a molecular beam nozzle, an excimer laser (Lumonics-510), a mass spectrometer (Extrel) and a vacuum chamber. The vacuum chamber was a cross of 10 in. outer di-

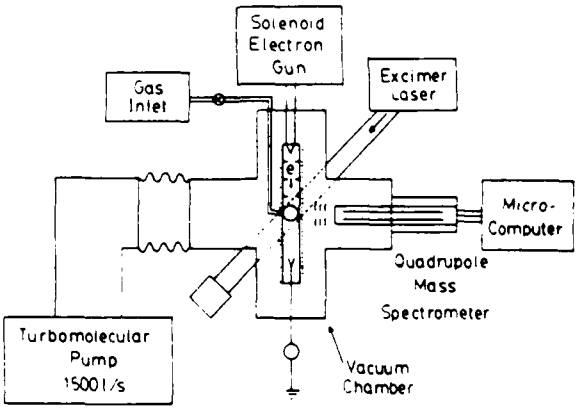

Fig. 1. Schematic diagram of apparatus.

0 009-2614/88/$ 03.50

ameter that was pumped by a 1500 ℓ/s turbomolecular pump (Balzer TSU-1500). The electron beam was produced by an electron gun for which the design was described before [1]. The electron beam was confined by a magnetic field generated by a solenoid. The cross sectional area of the electron beam was about 1 mm in diameter. The electron beam was extracted from a hot filament by applying a pulse voltage to the electron extractor. The molecular beam produced by flowing CH_3OH through a stainless steel nozzle which was 1.0 mm inner diameter and 4.0 mm long. The molecular beam crossed the electron beam at 90°. The cross sectional area of the laser beam was $1.19 \times 0.40 = 0.476$ cm^2 (the short side in vertical), and passed the electron–molecule interaction region in a direction perpendicular to the electron beam. The laser beam entered the vacuum chamber through a MgF_2 window, and the laser power was measured by a power meter (Scientech). The ions produced by electron-impact ionization were extracted by an electric field in the direction perpendicular to both the electron and the laser beams. The extraction electric field was established by two wire meshes separated 10 mm. The electron beam propagated along the central line between them. The extracted ions were accelerated to 300 V and were then focused into the entrance of the quadrupole mass spectrometer. The ions were detected by a channeltron.

The output pulses from the channeltron were amplified and counted by a 200 MHz photon counter system (Stanford Research System SR400). The fast photon counter was controlled by a microcomputer, which was also used to accumulate and to analyze the data. The counter gates, the excimer laser, and the electron beam pulses were triggered by a pulse generator (Hewlett–Packard) that provided double pulses with varied delay times. A multichannel scaler (Canberra) was also used to accumulate the ion signals as a function of time.

The pressure in the vacuum chamber was monitored by a cold cathode gauge installed about 50 cm from the electron–gas interaction region. The ultimate background pressure was about 3×10^{-8} mbar, and the gas pressure, typically used in the experiment, was in the 10^{-7} mbar range as measured by the cold cathode gauge. The gas pressure in the beam interaction region was measured to be about two orders of magnitude higher than the background pressure. This pressure gradient was determined by measuring the ion signals produced by admitting the gas through the molecular beam nozzle and through a side gas inlet that provided the same background pressure. The CH_3OH vapor was obtained from methanol (with purity of 99.9%) which was purified by liquid nitrogen.

2.2. Data acquisition procedure

The time sequence for laser pulse, double electron beam pulses and counter gates are depicted in fig. 2. The laser pulse (10 ns duration) served as the time reference ($t=0$). The electron beam pulses of duration, t_e, had a delay time, t_{ed}, from the laser pulse and a separation time, t_{es}. A two-channel counter was used with a duration of t_c for each gate. The delay time, t_{cd}, and the separation time, t_{cs}, of the counter gates could be set differently from the electron beam pulses. t_{cd} was set slightly longer than t_{ed}, and t_{es} was nearly equal to t_{es} of about 1 ms. The CH_3 radicals produced by laser excitation were subsequently ionized into CH_3^+ by the first electron beam pulse. The ionization threshold of $CH_3 \rightarrow CH_3^+ + e$ is at 9.84 eV [2]. The CH_3^+ ions were counted by the channel A. CH_3^+ can also be produced by dissociative electron-impact ionization of CH_3OH if the electron energy, E_e, is higher than the threshold for dissociative ionization of CH_3OH at 13.5 eV [3]. The channel A could include two signals – one from electron-impact ionization of CH_3 and the other from dissociative ionization of CH_3OH. The second electron pulse was far away from the laser pulse so that the radicals were pumped away from the interaction region, and the

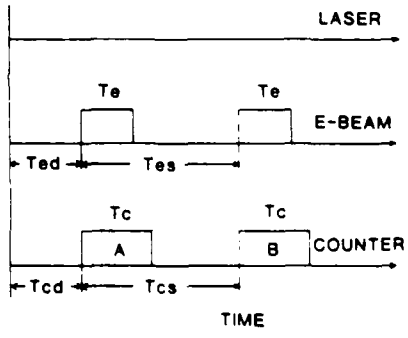

Fig. 2. Time sequence for laser pulse, double electron beam pulses, and counter gates.

signal of channel B is only due to electron-impact ionization of CH_3OH. The difference between channels A and B represents the signal due to electron-impact ionization of CH_3.

3. Results and discussion

3.1. Dependence of ion intensity on delay time

The CH_3^+ ion intensity was observed by channel A at varied delay time from laser pulse. The CH_3^+ ion intensity in the first 200 μs is larger than the background observed at long delay time. The additional laser-enhanced ion intensity is produced by electron-impact ionization of CH_3 and/or CH_3OH in electronically excited states. Since the photoabsorption cross section of CH_3OH around 193 nm is a continuum [4], laser excitation of CH_3OH mainly leads to dissociation, that is, the enhanced signals are mainly due to dissociation products, CH_3.

The decay time of the enhanced signal represents the time that the CH_3 radicals exist in the electron beam region. At the exit of the molecular beam nozzle, the molecular flow velocity in the electron beam region could be of the order of 10^3–10^4 cm/s. The time spent by slow radicals in the laser beam region is thus expected to be of the order of few hundred μs. The observed decay time (about 200 μs) of the enhanced signal is consistent with this expectation. A fraction of the radicals produced by photodissociation could carry high kinetic energies, depending on the potential surface that the dissociation process takes place. The exothermicity for photodissociation of CH_3OH into CH_3+OH at 193 nm is about 2.4 eV. A fraction of the radicals could acquire translational energy from the exothermic energy such that the radicals have high velocity. These fast radicals could move away from the electron beam region in a short time such that they are not detected.

3.2. Dependence of ion intensity on gas pressure, electron current, and laser power

The CH_3^+ ion intensity from ionization of the CH_3 radical by each electron beam pulse is given by

$$N_1 = K\sigma_e \int N_e n_1 \, dV, \qquad (1)$$

where K is a constant including ion extraction efficiency and ion detection efficiency, σ_e is the electron-impact ionization cross section, N_e is the number of electrons per unit area per electron pulse, n_1 is the radical concentration, and the integral is carried over the overlap region of the electron beam, laser beam, and molecular beam.

The radical concentration can be determined from the laser flux, I_ν, and the CH_3OH concentration, n_0, by

$$n_1 = I_\nu \sigma_\nu n_0, \qquad (2)$$

where σ_ν is the cross section for photodissociation of CH_3OH into CH_3+OH at 193 nm. The validity of this calculation is under the assumption that n_0 and I_ν are uniform over the interaction volume. Since the interaction volume is quite small, this assumption is reasonably good.

Substituting (2) into (1), we have

$$N_1 = KI_\nu \sigma_\nu \sigma_e \int N_e n_0 \, dV. \qquad (3)$$

This equation shows that the CH_3^+ ion intensity is proportional to laser power, electron beam current, and gas pressure. This assertion was tested by measuring the laser-enhanced signal as a function of these parameters. The results are shown in fig. 3. The data were measured with the time variables of $t_e = 300$ μs, $t_{ed} = 2$ μs, $t_{es} = 1.0$ ms, $t_e = 400$ μs, $t_{cd} = 20$ μs, and $t_{cs} = 960$ μs. For the pressure dependence shown in fig. 3a, the electron energy was 13.0 eV, the electron beam current was 75 nA averaged over 30 double pulses, and the laser flux was 30.0 mJ/cm^2 per pulse at 30 Hz. For the electron beam current dependence shown in fig. 3b, the electron energy was 13.0 eV, the gas pressure was 4.0×10^{-7} mbar, and the laser flux was 31.0 mJ/cm^2. For the laser flux dependence shown in fig. 3c, the electron energy was 15.0 eV, the gas pressure was 1.1×10^{-7} mbar, and the electron beam current was 645 nA. As expected, the laser-enhanced CH_3^+ ion intensity depends linearly on gas pressure, electron beam current, and laser flux. Those results support the assertion that the laser-enhanced signal is due to electron-impact ionization of CH_3.

3.3. Electron-impact ionization function of CH_3

The CH_3^+ ion intensity was measured as a func-

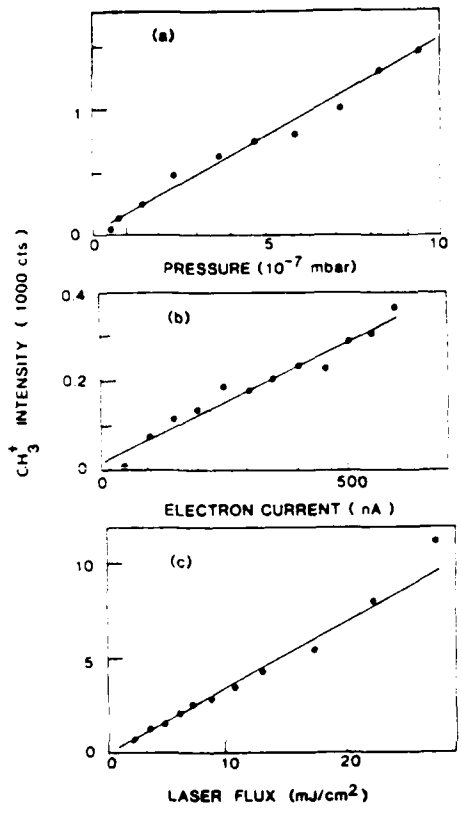

Fig. 3. Laser-enhanced CH_3^+ ion signals as a function of (a) gas pressure, (b) electron beam current, and (c) laser flux.

tion of electron energy as shown in fig. 4. The time variables were set at $t_c = 300$ μs, $t_{cd} = 2$ μs, $t_{cs} = 1.0$ ms, $t_c = 400$ μs, $t_{cd} = 20$ μs, and $t_{cs} = 960$ μs. The average laser flux was 29.9 mJ/cm^2 each pulse. The average electron beam current was 540 nA, and the gas pressure was 1.6×10^{-7} mbar.

As shown in fig. 4a, channel A has a constant signal more than channel B at electron energy lower than 10 eV. This additional signal is due to multiphoton dissociative ionization of CH_3OH by laser photons. At electron energy higher than 10 eV, the signal of channel A increases systematically with increasing electron energy. Channel B starts to show significant signal at about 14 eV. The difference between A and B is shown in fig. 4b, which represents the relative ionization cross section for the process

$$e + CH_3 \rightarrow CH_3^+ + 2e\,. \qquad (4)$$

The fluctuation of the data shown in fig. 4b is high

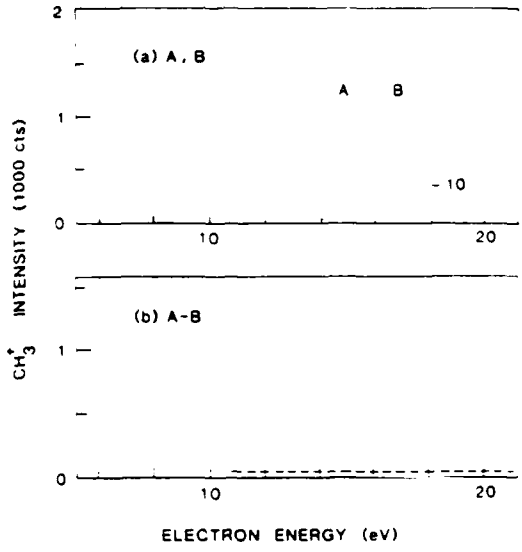

Fig. 4. (a) CH_3^+ ion intensities measured by channels A and B as a function of electron energy. (b) The difference between the signals of channels A and B.

at electron energy higher than 15 eV, because both channels A and B have large signals and their statistical uncertainties become high.

3.4. Electron-impact ionization cross sections of CH_3 and CH_3OH

The absolute electron-impact ionization cross section of CH_3 can be determined by comparing the CH_3^+ ion intensity observed from electron-impact ionization of CH_3 with other systems, for which the cross sections are known. The dissociative electron-impact ionization of CH_3OH,

$$e + CH_3OH \rightarrow CH_3^+ + OH + 2e, \qquad (5)$$

is chosen for the calibration. This system has the following advantages: (i) same CH_3^+ is detected so that the detection efficiency is essentially the same, and (ii) CH_3OH is the parent molecule of the radicals so that their spatial distribution in molecular beams are similar.

The CH_3^+ ion intensity produced by process (5) is given by

$$N_0 = K' \sigma_0 \int N_e n_0 \, dV\,, \qquad (6)$$

where K' is a constant that includes the extraction efficiency and the detection efficiency, and σ_0 is the electron-impact ionization cross section for process (5).

The ratio of N_1 and N_0 shown in eqs. (3) and (6) is thus equal to

$$N_1/N_0 = KI_\nu\sigma_\nu\sigma_e/K'\sigma_0, \quad (7)$$

or

$$\sigma_e = (N_1/N_0)\,(K'/K)\,\sigma_0/I_\nu\sigma_\nu, \quad (8)$$

where the spatial distributions of both CH_3 and CH_3OH are assumed to be the same.

The radical ionization cross section can thus be determined from the ion signals, the laser flux, and other parameters that are predetermined. The K' and K may be different due to different extraction efficiencies of the CH_3^+ ions that carry different kinetic energies. This difference is compensated by adjusting the extractor voltage, which was set at 8 V so that the extraction efficiencies for both systems were nearly in the saturation level. Under this condition, we assume that K' is equal to K. The photoabsorption cross section of CH_3OH at 193 nm is $\sigma_\nu = 3.0\times10^{-19}$ cm^2 [4]. The absorption is a dissociative process that may mainly lead to CH_3+OH. The electron-impact ionization cross sections of CH_3OH into various ion fragments were measured by the apparatus at the Jet Propulsion Laboratory [5]. The data at 100 eV are listed in table 1. The total ionization cross section, σ_T, which is the sum of all partial cross sections, is 4.70×10^{-16} cm^2. This is in good agreement with the value of 4.6×10^{-16} cm^2 measured by Durić, Cadez and Kurepa [6].

Table 1
Electron-impact ionization cross sections of CH_3OH at 100 eV

Ion species	Cross section (10^{-18} cm^2)
CH_3OH^+	113.16
CH_2OH^+	154.70
$CHOH^+$	12.35
CHO^+	93.45
CO^+	11.68
H_3O^+	0.49
H_2O^+	2.88
OH^+	2.02
O^+	1.20
CH_3^+	40.01
CH_2^+	6.50
CH^+	0.27
C^+	1.76
H_2^+	28.74
H^+	0.85
total (σ_T)	470.06

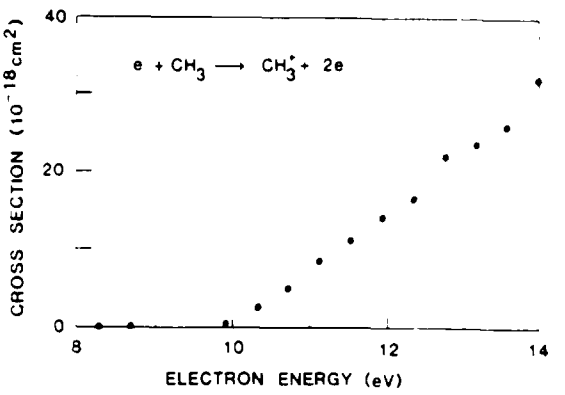

Fig. 5. Electron-impact ionization cross section of CH_3 as a function of electron energy.

Based on the above parameters as well as the measured ion signals and laser fluxes, the cross sections for the electron-impact ionization of CH_3 are shown in fig. 5. The experimental uncertainty due to the statistical fluctuation is less than 7%. The systematical error is difficult to determine, however, it is estimated to be within a factor 2 of the given value. The assumption that the spatial distribution of CH_3 radicals is the same as that of CH_3OH may cause a large uncertainty. Since the energy distribution of the CH_3 radicals depends on the method of radical production, the cross section obtained in this experiment is only an "apparent" value. It is of interest to compare this measured cross section with the values measured by other CH_3 sources. The current cross section of CH_3 is comparable with that of CD_3 measured by Baiocchi et al. [7] using a fast ion beam for the radical source.

4. Concluding remarks

The electron-impact ionization of CH_3 is investigated in the 10–22 eV region. The absolute ionization cross section in electron energy 10–14 eV is

determined by comparing the CH_3^+ ion intensity from electron-impact ionization of CH_3 with that of CH_3OH. The electron-impact ionization cross sections for dissociation of CH_3OH into various ion fragments at 100 eV are also reported.

Acknowledgement

This work is sponsored by the SDIO/IST and managed by ONR under Grant No. N00014-86-K-0558.

References

[1] E. Krishnakumar and S.K. Srivastava, J. Phys. B 21 (1988) 1055.

[2] G. Herzberg and J. Shoosmith, Can. J. Phys. 34 (1956) 523.
F.A. Edder, C. Giese, B. Steiner and M. Inghram, J. Chem. Phys. 36 (1962) 3292;
W.A. Chupka and C. Lifshitz, J. Chem. Phys. 48 (1968) 1109;
J.M. Williams and W.H. Hamill, J. Chem. Phys. 49 (1968) 4467;
F.P. Lossing and G.P. Semeluk, Can. J. Chem. 48 (1970) 955;
F.A. Houle and J.L. Beauchamp, J. Am. Chem. Soc. 101 (1979) 4067.

[3] L. Friedman, F.A. Long and M. Wolfsberg, J. Chem. Phys. 27 (1957) 613.

[4] J.B. Nee, M. Suto and L.C. Lee, Chem. Phys. 98 (1985) 147.

[5] E. Krishnakumar and S.K. Srivastava, unpublished.

[6] N. Duric, I. Cadez and M. Kurepa, private communication (1988).

[7] F.A. Baiocchi, R.C. Wetzel and R.S. Freund, Phys. Rev. Letters 53 (1984) 771.

Appendix B

Chemical Physics 114 (1987) 423–429
North-Holland, Amsterdam

FLUORESCENCE YIELDS FROM PHOTODISSOCIATIVE EXCITATION OF CHLOROMETHANES BY VACUUM ULTRAVIOLET RADIATION

L.C. LEE [1] and Masako SUTO

Department of Electrical and Computer Engineering, San Diego State University, San Diego, CA 92182, USA

Received 28 January 1987

The photoabsorption and fluorescence cross sections of chloromethanes were measured in the 105–220 nm region using synchrotron radiation as a light source. The fluorescence threshold for CCl_4 is at 152 nm with a maximum yield of 3% at 113 nm. The fluorescence results from the $CCl_2(\tilde{A}-\tilde{X})$ system. For $CHCl_3$, the fluorescence threshold is at 155 nm with a maximum yield of 0.6% at 110 nm. For CH_2Cl_2, the threshold is at 137 nm with a maximum yield of 0.35% at 107 nm. The fluorescence yield of CH_3Cl is very small with an upper limit of 0.02%. The photodissociation processes are discussed in accord with the fluorescence data observed. Vibrational structures in $CHCl_3$ and CH_2Cl_2 are observed and classified into progressions.

1. Introduction

Fluorescence from vacuum ultraviolet (VUV) photolysis of CCl_4 was recently observed and identified to be the $CCl_2(\tilde{A}^1B_1 \rightarrow \tilde{X}^1A_1)$ system [1]. The fluorescence excitation spectrum was reported [1], but the fluorescence cross section and quantum yield were not measured. It is of interest to measure the quantitative data, because they are important for understanding photodissociation processes as well as for practical applications. For example, the production yields of atomic Cl from photolysis of chlorine compounds are of interest in the study of atmospheric and intersteller chemistry and in the chemical etching of semiconductor materials. Photolyses of chloromethanes could be sources of CH_x ($x = 1$–3) radicals.

The absolute cross sections for photoabsorption and fluorescence of chloromethanes (CCl_4, $CHCl_3$, CH_2Cl_2 and CH_3Cl) were measured using synchrotron radiation as a light source. The absorption cross sections are used to compare, with previous values [1–5] that are somewhat controversal [1]. The quantitative fluorescence cross sections and quantum yields reported here are *new results*.

2. Experimental

The experimental arrangement has been described in previous papers [6,7]. In brief, synchrotron radiation produced from the electron storage ring at the University of Wisconsin was dispersed by a 1 m Seya vacuum monochromator. The absorption cross section was measured by the attenuation of light source by molecules in a gas cell of 39.2 cm path length. The experimental uncertainty for the absorption cross section is estimated to be within 10% of the given value. The VUV light intensity was measured by a combination of sodium salicylate coated on a window and a photomultiplier tube (PMT). The fluorescence was observed in a direction perpendicular to the light source by a PMT (EMI 9558QB), for which the response was about constant in the 180–400 nm region and then gradually decreased to nearly zero at about 800 nm. The absolute fluorescence cross section was obtained by comparing the fluorescence intensity with the OH(A–X) fluorescence produced from photodissociative excitation of

[1] Also at: Department of Chemistry, San Diego State University, San Diego, CA 92182, USA.

0301-0104/87/$03.50

H_2O, for which the fluorescence cross section is known [6,7]. The PMT response was not corrected in the absolute fluorescence measurement. The fluorescence cross section could be higher than the given value by a factor of two, if the correction for the PMT response is made.

Liquid CCl_4 was supplied by EM Industries with a stated purity of better than 99.9%. Liquid $CHCl_3$ and CH_2Cl_2 were supplied by Fisher Scientific with purities of better than 99.7% and 99.9%, respectively. These liquids were degassed by cooling down to solid with liquid N_2. The samples were repeatedly purified such that the absorption due to possible impurities, such as O_2, was not observed in the absorption spectra. CH_3Cl was supplied by Matheson with a purity of better than 99.5%, and was used in the experiment as delivered.

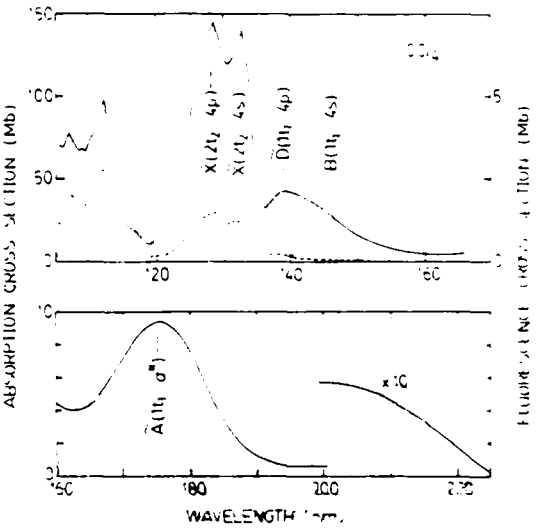

Fig. 1. Photoabsorption (———) and fluorescence (---) cross sections of CCl_4 measured with a monochromator resolution of 0.2 nm.

3. Results and discussion

3.1. CCl_4

The absorption cross section of CCl_4 in the 105–220 nm region is shown in fig. 1, which was measured with a monochromator resolution of 0.2 nm. The absorption bands have been assigned to Rydberg states as discussed by several investigators [3,8], and the assignment given by Robin [8] is indicated in fig. 1. The discrepancy between the earlier absorption data has been pointed out by Ibuki et al. [1]. The current result agrees within experimental uncertainty with the data of Russell et al. [3] in the 110–200 nm region, but it is higher than the data of Ibuki et al. by about 40% in the 110–135 nm region.

The cross section for the production of fluorescence from photodissociative excitation of CCl_4 is shown in fig. 1. The fluorescence was observed simultaneously with the absorption measurement. The fluorescence has been attributed to the $CCl_2(\tilde{A}-\tilde{X})$ system [1]. The structure shown in the fluorescence cross section is very similar to that of the absorption cross section.

The fluorescence yield, which is defined as the ratio of fluorescence cross section to absorption cross section, is shown in fig. 2a. The fluorescence yield starts at 152 nm, increases to a plateau of about 1% at 130 nm, and then reaches a maximum of about 3% at 113 nm.

The fluorescence yield is a measure of the interaction strength between the initial excited state and the repulsive state that produces the emitting species. The vertical energy of the repulsive state

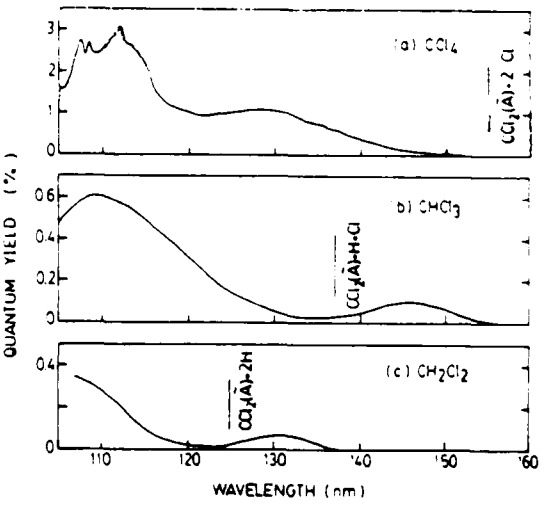

Fig. 2. Fluorescence quantum yields of (a) CCl_4, (b) $CHCl_3$, and (c) CH_2Cl_2. The calculated thresholds for the dissociation processes that produce CCl_2 ($\tilde{A}-\tilde{X}$) fluorescence are indicated.

can be determined from the wavelength at the maximum fluorescence yield. The first repulsive state, which has a maximum fluorescence yield at 128 nm (vertical energy of 9.7 eV), may dissociate into $CCl_2(\tilde{A}) + Cl_2$. The threshold wavelength for this process is at 224 nm. The second repulsive state, which has a maximum fluorescence yield at 113 nm (vertical energy of 11.0 eV), likely dissociates into $CCl_2(\tilde{A}) + 2Cl$. The threshold for this process is at 155 nm. The threshold wavelengths are calculated using the heats of formation for CCl_4, CCl_2, and Cl of -22.42, 56.7, and 28.587 kcal/mol, respectively [9,10], the dissociation energy of $D_0(Cl-Cl) = 2.479$ eV [11], and the excitation energy for the $CCl_2(\tilde{A}\ ^1B_1(0, 0, 0) \leftarrow \tilde{X}\ ^1A_1(0, 0, 0))$ transition of 2.1 eV [12].

3.2. $CHCl_3$

3.2.1. Photoabsorption

The photoabsorption cross section of $CHCl_3$ is shown in fig. 3, which was measured with a monochromator resolution of 0.4 nm. The current result is generally higher than the data of Russell et al. [3] by about 25%, and significantly higher than the data of Lucazeau and Sandorfy [2].

The absorption bands of $CHCl_3$ have been previously assigned to Rydberg transitions [3,8], and the assignment given by Robin [8] is indicated in fig. 3. In addition to the broad absorption bands, weak vibrational structures were observed in the absorption spectrum. The absorption spectrum measured with a monochromator resolution of 0.04 nm is shown in fig. 4. The first vibrational progression is superimposed on the 3e → 4p Rydberg transition, indicating that the vibrational progression may be a member of the Rydberg series converging to the ^2E ion state of $CHCl_3$. The absorption spectra for the $\tilde{D}(1a_2 \rightarrow 4p)$ and $\tilde{X}(3e \rightarrow 4p)$ Rydberg transitions are very similar to the photoelectron spectra of the $^2A_2$ and ^2E ion states of $CHCl_3^+$ [13,14]. This similarity further suggests that the first level of the vibrational progression at 136.61 nm likely converges to the threshold of the ^2E ion state which is at 11.6 eV [13,14]. Based on this assumption, the effective quantum number for the Rydberg transition is calculated by the Rydberg formula,

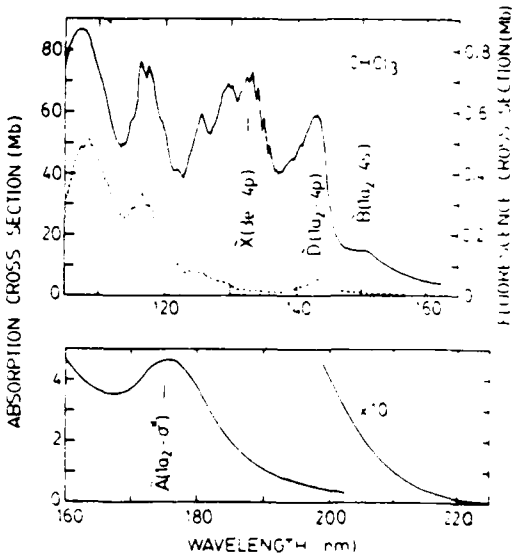

Fig. 3. Photoabsorption (———) and fluorescence (---) cross sections of $CHCl_3$ measured with a monochromator resolution of 0.4 nm.

$$\nu = \nu_0 - 109737/n^{*2}, \quad (1)$$

where $\nu_0 = 93560\ cm^{-1}$ is the threshold potential energy of the ^2E ion state [13,14]. The effective quantum numbers, wavelengths, wave numbers, and vibrational frequencies for the tentatively as-

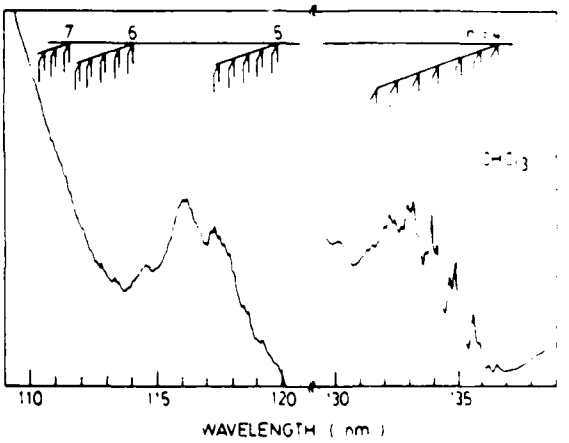

Fig. 4. Photoabsorption spectrum of $CHCl_3$ measured with a monochromator resolution of 0.04 nm. The wavelength positions for the vibrational progressions of tentatively assigned Rydberg series are indicated.

signed vibrational progressions of other Rydberg members are listed in table 1 as well as indicated in fig. 4. The wavelength is calibrated against the known absorption spectra of CH_3Cl [15] and H_2O [16] which were measured in the same experiment. The uncertainty for the wavelength calibration is estimated to be 0.1 nm for the absolute value and 0.02 nm for the relative value.

As listed in table 1, the average frequency for the vibrational progressions is about 410 cm^{-1}. This value is close to the ν_3 frequency (CCl_3 symmetrical deformation mode) of the ground state of $CHCl_3$ (363 cm^{-1}) [17,18]. As shown in fig. 4, each vibrational band has a double peak with a frequency separation of about 120 cm^{-1}.

3.2.2. Fluorescence

The cross section for the production of fluorescence from photodissociative excitation of $CHCl_3$ was simultaneously measured with the absorption cross section. The result is shown in fig. 3. The fluorescence cross section is used to calculate the quantum yield as shown in fig. 2b. The fluorescence yield starts at 155 nm, and then reaches two maxima of 0.1% and 0.6% at 146 and 110 nm, respectively. The first band likely corresponds to a repulsive state (with a vertical energy of 8.5 eV) that dissociates into

$$CHCl_3 \rightarrow CCl_2(\tilde{A}) + HCl. \quad (2)$$

The threshold wavelength for this process is 268 nm, where the heats of formation of −22.019 and −23.49 kcal/mol for HCl and $CHCl_3$ [9,10], respectively, are used for the calculation.

The second fluorescence band likely corresponds to a repulsive state (with a vertical energy of 11.3 eV) that dissociates into

$$CHCl_3 \rightarrow CCl_2(\tilde{A}) + H + Cl. \quad (3)$$

The threshold for this process is 137 nm, where the dissociation energy of $D_0(H\text{-}Cl) = 4.434$ eV [11] is used for the calculation. The calculated threshold wavelength coincides very well with the observed threshold as in fig. 2b.

Table 1
The effective quantum numbers, n^* wavelengths, λ, wave numbers, ν, and vibrational frequencies, $^1\Delta\nu$, for the tentatively assigned vibrational progressions of the Rydberg series converging to the ^2E ion state of $CHCl_3^+$

n	n^*	v	λ (nm)	ν (cm^{-1})	$\Delta\nu$ (cm^{-1})
4	2.32	0	136.61	73201	
		1	135.86	73605	404
		2	135.06	74041	436
		3	134.08	74582	541
		4	133.36	74985	403
		5	132.42	75517	432
		6	131.71	75924	407
5	3.29	0	119.84	83444	
		1	119.24	83864	420
		2	118.66	84274	410
		3	118.07	84696	422
		4	117.51	85099	403
6	4.32	0	114.05	87681	
		1	113.49	88113	432
		2	112.94	88543	430
		3	112.42	88952	409
		4	111.89	89373	421
7	5.28	0	111.57	89630	
		1	110.06	90041	411
		2	110.54	90464	423
0				93560	

3.3. CH_2Cl_2

3.3.1. Photoabsorption

The photoabsorption cross section of CH_2Cl_2 measured with a monochromator resolution of 0.2 nm is shown in fig. 5. The current result agrees very well with the data of Russell et al. [3]. The absorption bands in the 130–200 nm region have been assigned to Rydberg transitions [3,8]. The assignment given by Robin [8] is indicated in fig. 5.

Vibrational structure appears in the absorption spectrum at wavelengths shorter than 145 nm. An attempt to classify these absorption bands into Rydberg series is not successful, instead, six vibrational progressions are classified as shown in fig. 6, which was measured with a monochromator resolution of 0.04 nm. The wavelengths, wave numbers, and vibrational frequencies for the tentatively classified vibrational progressions are listed in table 2. The vibrational progressions I and II have been observed by Zobel and Duncan

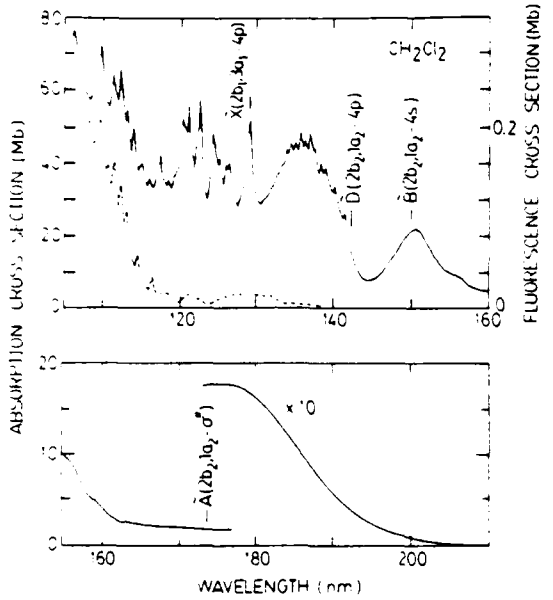

Fig. 5. Photoabsorption (———) and fluorescence (---) cross sections of CH_2Cl_2 measured with a monochromator resolution of 0.2 nm.

[19]. The progressions I, II, and VI have an average vibrational frequency of about 680 cm^{-1}, which is close to the ν_3 frequency (CCl_2 symmetrical stretching mode) of the ground state of CH_2Cl_2 (717 cm^{-1}) [18]. The vibrational progressions III, IV, and V have an average vibrational frequency of about 1000 cm^{-1}, which is close to

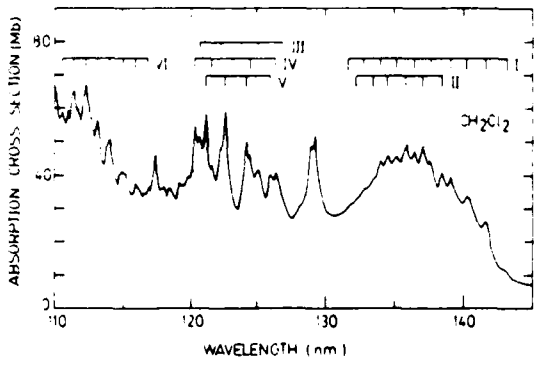

Fig. 6. Photoabsorption spectrum of CH_2Cl measured with a monochromator resolution of 0.04 nm. The wavelength positions for the tentatively assigned vibrational profgressions are indicated.

the ν_5 frequency (CH_2 twisting mode) of the ground state of CH_2Cl_2 (1153 cm^{-1}) [18].

3.3.2. Fluorescence

The fluorescence cross section of CH_2Cl_2, which is simultaneously measured with the ab-

Table 2
Wavelengths, λ, wavenumbers, ν, and vibrational frequencies $\Delta\nu$, for the tentatively assigned vibrational progressions of CH_2Cl_2

Progression	v	λ (nm)	ν (cm^{-1})	$\Delta\nu$ (cm^{-1})
I	0	143.00	69930	
	1	141.59	70626	696
	2	140.31	71270	644
	3	139.10	71890	620
	4	137.72	72611	621
	5	136.45	73287	676
	6	135.23	73948	661
	7	133.97	74644	696
	8	132.76	75324	680
	9	131.58	75999	675
II	0	138.43	72239	
	1	137.09	72945	706
	2	135.81	73632	687
	3	134.53	74333	701
	4	133.29	75024	691
	5	132.09	75706	682
III	0	126.79	78871	
	1	125.10	79936	1065
	2	123.74	80815	879
	3	122.14	81873	1058
	4	120.60	82919	1046
IV	0	126.35	79145	
	1	124.40	80386	1241
	2	122.99	81307	921
	3	121.53	82284	977
	4	120.26	83153	869
V	0	125.82	79479	
	1	124.11	80574	1095
	2	122.56	81593	1019
	3	121.10	82576	983
VI	0	116.81	85609	
	1	115.89	86289	680
	2	114.93	87009	720
	3	114.01	87712	703
	4	113.16	88370	658
	5	112.29	89055	685
	6	111.40	89767	712
	7	110.59	90424	657
	8	109.81	91066	642

sorption cross section, is shown in fig. 5. The fluorescence yield determined from the fluorescence cross section is shown in fig. 2c. Similar to CCl_4 and $CHCl_3$, the fluorescence yield shows two bands with maxima of 0.06% and 0.35% at 131 and 107 nm, respectively. The first band likely corresponds to a repulsive state (with a vertical energy of 9.5 eV) that dissociates into

$$CH_2Cl_2 \rightarrow CCl_2(\tilde{A}) + H_2. \quad (4)$$

The threshold of this process is calculated at 226 nm, using heat of formation of −21.19 kcal/mol for CH_2Cl_2 [9,10]. This calculated threshold wavelength is much longer than the fluorescence threshold wavelength observed at 137 nm.

The second band likely corresponds to the process

$$CH_2Cl_2 \rightarrow CCl_2(\tilde{A}) + 2H. \quad (5)$$

for which the threshold wavelength is 125 nm, where the dissociation energy of H_2 (4.4781 eV [11]) is used for the calculation. The calculated threshold for this second fluorescence band coincides with the observed threshold as shown in fig. 2c. The wavelength for the maximum yield of this band may occur at a wavelength shorter than 106 nm.

The $CH_2(\tilde{b}\,^1B_1 - \tilde{a}\,^1A_1)$ emission, which has been observed from the photodissociative excitation of CH_4 [20], may be produced from the photoexcitation process

$$CH_2Cl_2 \rightarrow CH_2(\tilde{b}) + Cl_2. \quad (6)$$

The wavelength threshold for this process is expected to be 130 nm, as calculated from the heat of formation of 92.25 kcal/mol for CH_2 [9,10] and the excess energy of 4.63 eV required for the production of the $CH_2(\tilde{b}-\tilde{a})$ emission. This excess energy is assumed to be equal to the excess energy that produces the same emission from the excitation process of $CH_4 \rightarrow CH_2 + H_2$ [20]. The fluorescence yield for the $CH_2(\tilde{b} \rightarrow \tilde{a})$ emission is, however, expected to be quite small because the fluorescence yield for CH_3Cl is very small as discussed below.

3.4. CH_3Cl

The absorption cross section of CH_3Cl measured with a monochromator resolution of 0.04 nm is shown in fig. 7. The current result agrees with the data of Russell et al. [3] within experimental uncertainty. The absorption bands have been assigned to Rydberg transitions by several investigators [3,8,15,21]. The assignment given by Robin [8] is indicated in fig. 7. The sharp absorption bands have been classified into Rydberg series by Hochmann et al. [21].

The relative cross section for the production of fluorescence from photodissociative excitation of CH_3Cl is shown in fig. 7, where the data were measured with a resolution of 0.7 nm. The upper limit for the fluorescence cross section is estimated

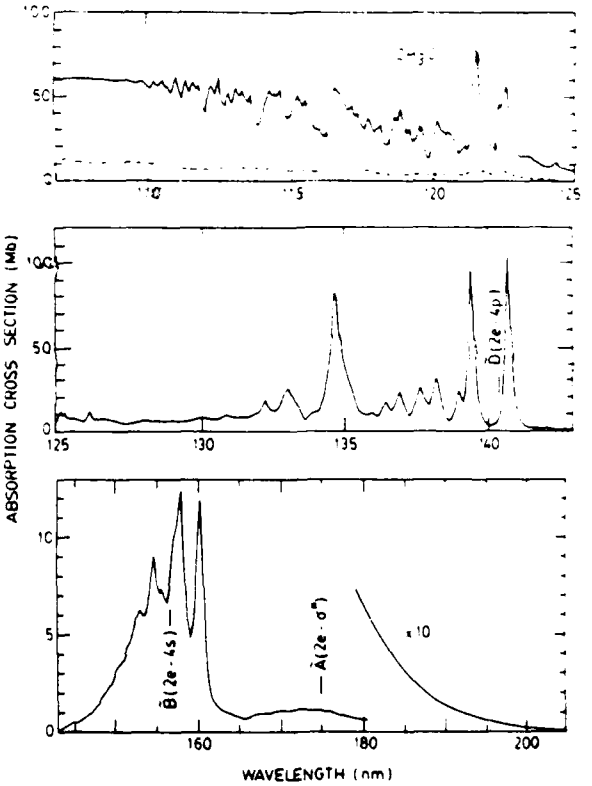

Fig. 7. Photoabsorption (———) and relative fluorescence (---) cross sections of CH_3Cl. The monochromator resolutions were 0.04 nm for the absorption and 0.7 nm for the fluorescence. The upper limit for the fluorescence cross section is estimated to be 10^{-20} cm^2.

to be 10^{-20} cm^2. The fluorescence cross section is quite small when compared with other chloromethane molecules. The fluorescence yield is smaller than 0.02% for the entire wavelength region studied. The fluorescence may mainly consist of the $CH_2(\tilde{b}-\tilde{a})$ emission, which is produced from the process,

$$CH_3Cl \rightarrow CH_2(\tilde{b}) + HCl. \quad (7)$$

The wavelength threshold for this process is 147 nm as calculated from the heats of formation of -22.019 and -18.1 kcal/mol for HCl and CH_3Cl, respectively [9,10], and the excess energy of 4.63 eV for the production of the $CH_2(\tilde{b}-\tilde{a})$ emission [20]. This calculated threshold is longer than the observed fluorescence threshold of about 124.5 nm.

4. Concluding remarks

The absorption and fluorescence cross sections of CCl_4, $CHCl_3$, CH_2Cl_2, and CH_3Cl are measured in the 105–220 nm region, and used to determine the fluorescence quantum yields. In general, the spectrum of each fluorescence yield shows two maxima, indicating that the fluorescence is produced by two repulsive states. The wavelength at the maximum fluorescence yield is used to determine the vertical energy of the repulsive state.

Robin [8,22] has assigned the intense energy loss band at 81000 cm^{-1} in the electron impact spectrum of CCl_4 to the $\sigma \rightarrow \sigma^*$ transition. This transition may correspond to the first fluorescence band of CCl_4 that has a maximum yield of about 1% at 130 nm as shown in fig. 2a. Similarly, the first fluorescence bands of $CHCl_3$ and CH_2Cl_2 as shown in figs. 2b and 2c could be assigned to the same transition.

Acknowledgement

The authors wish to thank the staff of the Synchrotron Radiation Center of the University of Wisconsin for their delicate operation of the facility. The synchrotron radiation facility is supported by the NSF under Grant No. DMR-44-21888. This work is based on the work supported by the NSF under Grant No. ATM-8412618 and CBT-8518555, the NASA under Grant No. NAGW-319, and the ONR under Grant No. N00014-86-K-0558.

References

[1] T. Ibuki, N. Takahashi, A. Hiraya and K. Shobatake, J. Chem. Phys. 85 (1986) 5717.
[2] G. Lucazeau and C. Sandorfy, J. Mol. Spectry. 35 (1970) 214.
[3] B.R. Russell, L.O. Edwards and J.W. Raymonda, J. Am. Chem. Soc. 95 (1973) 2129.
[4] G.C. Causley and B.R. Russell, J. Electron Spectry. 11 (1977) 383.
[5] H. Tsubomura, K. Kimura, K. Kaya, J. Tanaka and S. Nagakura, Bull. Chem. Soc. Japan 37 (1964) 417.
[6] L.C. Lee, J. Chem. Phys. 72 (1980) 4334.
[7] L.C. Lee and M. Suto, Chem. Phys. 110 (1986) 161.
[8] M.B. Robin, Higher excited states of polyatomic molecules, Vols. 1, 2 (Academic Press, New York, 1974).
[9] H. Okabe, Photochemistry of small molecules (Wiley, New York, 1978).
[10] D.R. Stull and H. Prophet, eds., JANAF thermochemical tables, 2nd Ed., NSRDS-NBS 37 (1971).
[11] K.P. Huber and G. Herzberg, Molecular spectra and molecular structure, Vol. 4. Constants of diatomic molecules (Van Nostrand–Reinhold, New York, 1979).
[12] D.A. Predmore, A.M. Murray and M.D. Harmony, Chem. Phys. Letters 110 (1984) 173.
[13] A.W. Potts, H.J. Lempka, D.G. Streets and W.C. Price, Phil. Trans. Roy. Soc. London A 268 (1970) 59.
[14] R.N. Dixon, J.N. Murrell and B. Narayan, Mol. Phys. 20 (1971) 611.
[15] S. Felps, P. Hochmann, P. Brint and S.P. McGlynn, J. Mol. Spectr. 59 (1976) 355.
[16] H.T. Wang, W.S. Felps and S.P. McGlynn, J. Chem. Phys. 67 (1977) 2614.
[17] G. Herzberg, Infrared and Raman spectra of Polyatomic molecules, Vol. 2 (Van Nostrand, New York, 1945).
[18] T. Shimanouchi, Tables of molecular vibrational frequencies, Consolidated Vol. 1, NSRDS-NBS 39 (1972).
[19] C.R. Zobel and A.B.F. Duncan, J. Am. Chem. Soc. 77 (1955) 2611.
[20] L.C. Lee and C.C. Chiang, J. Chem. Phys. 78 (1983) 688.
[21] P. Hochmann, P.H. Templet, H.T. Wang and S.P. McGlynn, J. Chem. Phys. 62 (1975) 2588.
[22] M.B. Robin, Higher excited states of polyatomic molecules (Academic Press, New York, 1985) pp. 109–110.

Appendix C

International Journal of Mass Spectrometry and Ion Processes, 88 (1989) 267–276
Elsevier Science Publishers B.V., Amsterdam – Printed in The Netherlands

DISSOCIATIVE IONIZATION OF LASER EXCITED N_2^* BY ELECTRON IMPACT

D.P. WANG and L.C. LEE

Department of Electrical and Computer Engineering, San Diego State University, San Diego, CA 92182 (U.S.A.)

S.K. SRIVASTAVA

Jet Propulsion Laboratory, California Institute of Technology, Pasadena, CA 91109 (U.S.A.)

(First received 5 August 1988; in final form 4 October 1988)

ABSTRACT

N_2 molecules were excited by ArF (193 nm) laser photons and then dissociatively ionized by electron impact. The laser-enhanced N^+ ion intensity is linearly dependent on laser power, N_2 pressure and electron beam current. The enhanced ion signal is attributed to the electron-impact ionization of laser excited N_2^* in the $A^3\Sigma_u^+$ state. The excitation function for the production of N^+ ions by electron impact on N_2^* was measured at 17–32 eV.

INTRODUCTION

Excited N_2^* molecules are quite abundant in N_2 discharge media and they have a substantial effect on discharge characteristics [1–5]. Electron excitation function of N_2^* is thus of interest for the understanding of discharge phenomena. However, very little data are available for the excited states, in contrast to the ground state which has been extensively studied [6–14]. The electron-impact ionization of N_2^* (A) has been investigated once by Armentrout et al. [15] using a charge transfer neutralization beam of N_2^+ with NO. The study of excited states is difficult because the excited species is chemically active and its concentration is usually limited to a small quantity.

In this experiment, the excited N_2^* species were produced by ArF (193 nm) laser irradiation. The excited species are presumably in the $A^3\Sigma_u^+$ metastable state of which the lifetime is about 1 s [16]. The photo-absorption spectrum of the $N_2(A \leftarrow X)$ system has been investigated by Shemansky [17]. The photo-absorption cross-section of N_2 at 193 nm is expected to be small; however, the excimer laser intensity was so strong that a reasonable

0168-1176/89/$03.50

amount of excited species could be prepared for the experiment. The probability for excitation of N_2 into the $A^3\Sigma_u^+$ state could be of the order of 10^{-7} at a typical laser power density of 40 mJ cm^{-2} and an assumed average photo-absorption cross-section of 10^{-24} cm^2. The excitation function for the production of N^+ from electron-impact ionization of excited N_2^* is reported in this paper.

EXPERIMENTAL

Apparatus

A schematic diagram of the experimental apparatus is given in Fig. 1. The apparatus consists of an electron beam, a molecular beam nozzle, an excimer laser (Lumonics-510) and a quadrupole mass spectrometer [18]. The vacuum chamber was pumped by a turbomolecular pump (Balzer TSU-1500). The background vacuum pressure was about 5×10^{-8} mbar. The electron gun and ion extraction system were similar to the design reported in a previous paper [19]. Electrons were produced by a hot filament and confined by a solenoid magnetic field. Ions, after mass selection by the quadrupole mass spectrometer, were detected by a channeltron. The output pulses from the channeltron were amplified and counted by a 200-MHz photon counter system (Stanford Research System SR400). The fast photon counter was controlled by a microcomputer, which was also used to accumulate and to analyze the data. The counter gates, the excimer laser and the electron beam pulses were triggered by a pulse generator that provided double pulses with varied delay times.

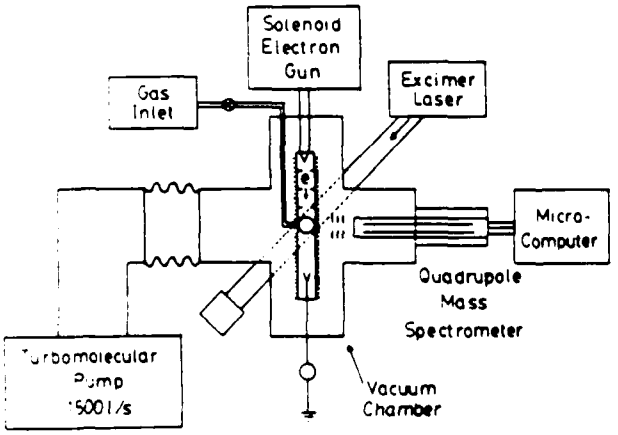

Fig. 1. Schematic diagram of the experimental set-up.

The gas was introduced into the vacuum chamber through an adjustable leak valve. The pressure between the leak valve and the vacuum chamber was measured by a capacitance manometer. The pressure in the vacuum chamber was monitored by a cold cathode gauge installed about 50 cm from the electron-gas interaction region. The gas pressure typically used in the experiment was in the 10^{-7} mbar range as measured by the cold cathode gauge. The gas pressure in the interaction region of laser and electron beams was measured to be about two orders of magnitude higher than the background pressure. The N_2 gas purity was better than 99.99%.

The laser beam diameter was reduced by an iris aperture of 0.32 cm. MgF_2 windows were placed on the vacuum chamber for laser transmission. The laser power was monitored by a power meter (Scientech). Laser power attenuation was accomplished by placing quartz and sapphire plates in the laser beam path. The whole system was tested with inert gases. The electron excitation functions of inert gases (Ne, Ar and Kr) are in good agreement with published data over the energy range 5-300 eV [20]. The electron beam energy, E_e, was calibrated by ionization thresholds of inert gases. The energy resolution was about 0.5 eV.

Data acquisition procedure

The time sequences for laser pulse, double electron beam pulses and counter gates are depicted in Fig. 2. The laser pulse (10-ns duration) served as the time reference ($t = 0$). The double electron beam pulses had a delay time, t_{ed}, from the laser pulse and a separation time, t_{es}, between the pulses. Each pulse had a duration time, t_e, that was variable. A two channel counter was used with a duration of t_c for each gate. The delay time, t_{cd}, and the

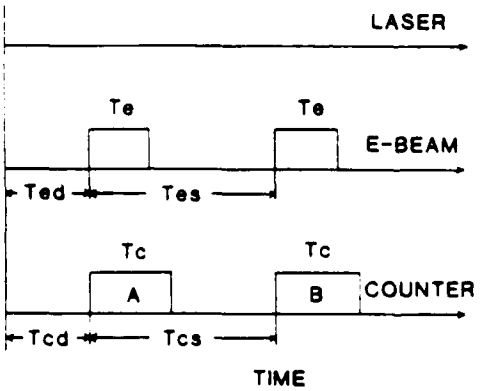

Fig. 2. Time sequence for laser pulse, electron beam pulses and counter gates. Typically, $t_{ed} = 2$ μs, $t_e = 100$ μs, $t_{es} = 1$ ms, $t_{cd} = 20$ μs, $t_c = 200$ μs and $t_{cs} = 960$ μs.

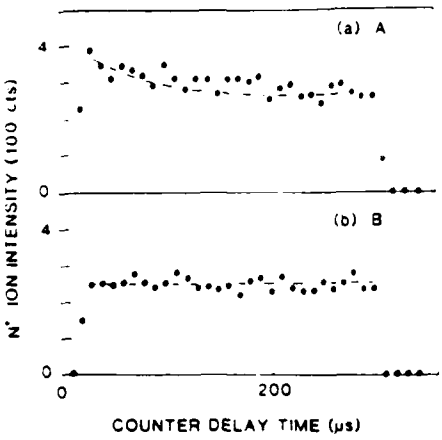

Fig. 3. N^+ ion intensity as a function of the delay time of the counter gate. (a) Signal accumulated by channel A that includes signals from both N_2 and N_2^*. (b) signal accumulated by channel B that is only due to N_2. The electron energy was 30 eV.

separation time, t_{cs}, of the counter gates could be set differently from the electron beam pulses. t_{cd} was set slightly longer than t_{ed}, and t_{cs} was nearly equal to t_{es}. Typically, $t_{ed} = 2$ μs, $t_e = 100$ μs, $t_{es} = 1$ ms, $t_{cd} = 20$ μs, $t_c = 200$ μs and $t_{cs} = 960$ μs.

The N^+ ions produced by electron excitation of N_2 were observed. Channel A of the counter collected the N^+ ion signals produced by electron-impact ionization of both N_2 and N_2^*. For channel B, the metastable N_2^* had already moved out of the collision region so this channel collected only the ion signal from N_2. Channel B is typically set about 1 ms later than channel A so that the laser-enhanced signal does not appear in channel B (see Fig. 3 for further discussion). The difference between the ion intensities measured by the A and B channels represents the difference of the dissociative electron-impact ionization cross-sections of N_2^* and N_2. The present procedure has the advantage that the data are taken in a short time after each laser pulse so that the laser-enhanced signals are not seriously affected by the fluctuations of gas pressure, electron beam current and detection efficiency, which may change in a long time scale. The signals were observed at varied delay times, laser powers, gas pressures, electron beam currents and electron energies.

RESULTS AND DISCUSSION

The laser-enhanced N^+ ion signals were observed as a function of the counter delay time (t_{cd}) as shown in Fig. 3, where the signals of channel A are shown in (a), and those of channel B in (b). The laser was operated at 30

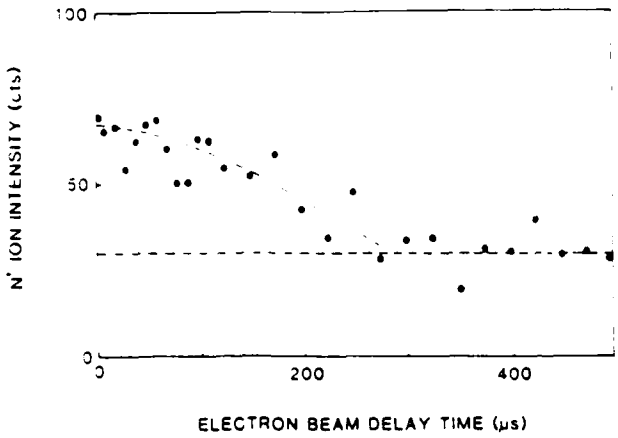

Fig. 4. N^+ ion intensity from channel A as a function of electron beam delay time. The electron energy is 22.0 eV.

Hz with an energy flux of 28 mJ cm^{-2} for each pulse. Each point of the signals was accumulated by 1500 laser pulses. The N_2 pressure measured by the cold cathode gauge was 1.2×10^{-7} mbar. The average electron beam current was 60 nA with an electron energy of 30.0 eV. The electron beam pulses were set at $t_e = 100$ μs, $t_{ed} = 2$ μs and $t_{es} = 1$ ms. The counter gates were set at $t_c = 10$ μs and $t_{cs} = 1$ ms, and t_{cd} was scanned with a 10-μs increment.

As shown in Fig. 3, the signals start to appear at $t_{cd} = 20$ μs. This delay time represents the time of flight of the N^+ ions over the distance (about 43 cm) between the electron beam and the ion detector. The ion signals of A decrease to a constant level of B at about 200 μs. The channel A has a total of 1570 counts more than that of B, namely, about one ion count for each laser pulse. This signal level is expected if the average photo-absorption cross-section is of the order of 10^{-24} cm^2, the N_2 concentration in the electron beam region is 10^{12} molecules cm^{-3}, and the dissociative ionization cross-section of the excited state is of the order of 10^{-15} cm^2. These parameters are within reasonable ranges of expectation.

The lifetime of the excited species in the electron beam region was further measured by scanning the electron beam delay time. The N^+ ion intensity as a function of electron beam delay time (t_{ed}) is shown in Fig. 4. In this measurement, only a single electron pulse was generated after each laser pulse. The electron pulse duration was set at $t_e = 10$ μs and t_{ed} was scanned at a 10-μs increment. The counter gate of channel A was set at $t_{cd} = 20$ μs and $t_c = 800$ μs. The N_2 pressure was 2.7×10^{-7} mbar. The laser energy flux was 30 mJ cm^{-2}. The electron beam current was 20 nA with an electron energy of 22.0 eV. The ion signals decrease to a constant level at about 200

μs; this time duration is consistent with the data of Fig. 3. The constant background signal was contributed mainly from the mulitphoton ionization of N_2.

Data of both Figs. 3 and 4 show that the excited species existing in the electron beam region are quite long, indicating that the excited species are in metastable states. There are only two excited species, N_2^* (A, $v = 1$) and N_2^* (X, $v = 26$), that can be produced by the laser (193 nm) excitation. The photo-excitation of $N_2(X)$ to $N_2^*(A)$ has been observed [17] but the vibrational excitation is not observed, suggesting that $N_2^*(A)$ is produced more favorably than $N_2^*(X)$. Thus, the excited species is mostly in the $N_2^*(A)$ state, although the possibility for the highly vibrationally excited $N_2^*(X)$ is not ruled out. The radiative lifetime of $N_2^*(A)$ is about 1 s [16]. The quenching rate constant of $N_2^*(A)$ by N_2 is about 10^{-12} cm^3 s^{-1} [21]: thus, the quenching rate is about 0.2 s^{-1} for a N_2 pressure of 10^{-5} mbar. The loss of $N_2^*(A)$ by radiation and quenching is much smaller than the diffusion loss. The observed lifetime represents the residence time of the excited species in the electron beam region. The molecular beam after the nozzle is estimated to have a flow velocity in the order of 10^3–10^4 cm s^{-1}. The time for the excited species spent in the electron beam region is thus expected to be of the order of hundred microseconds as observed.

The electron energy of 22 V for producing the laser-enhanced N^+ ion signals shown in Fig. 4 is below the dissociative ionization threshold of N_2 of 24.3 eV [16]. Therefore, the observed ions are clearly not produced by electron-impact ionization of N_2 in the ground state, but in the excited state. The laser-enhanced N^+ ion intensity, n^+, is expected to be

$$n^+ = kn^* I_e \tag{1}$$

$$= k' n I \sigma_0 I_e \tag{2}$$

where k and k' are proportional constants, n^* is the density of excited species, n is the N_2 gas density, I is the laser photons per cm^2 per pulse, σ_0 is the cross-section for the production of the excited state by the laser excitation, and I_e is the electron beam current.

The relationship of Eq. 2 is checked by measuring the laser-enhanced ion intensities at varied laser fluxes, gas pressures and electron beam currents. The laser power dependence of the laser-enhanced ion signal is shown in Fig. 5a. The data were taken at an average electron beam current of 196 nA, electron pulse duration of 100 μs, electron energy of 22.1 eV and N_2 gas pressure of 1.0×10^{-7} mbar. The linear dependence of the laser-enhanced ion intensity on laser flux checks well with Eq. 2.

The dependence of the laser-enhanced ion intensity on the gas pressure is shown in Fig. 5b. The data were taken at an average electron beam current

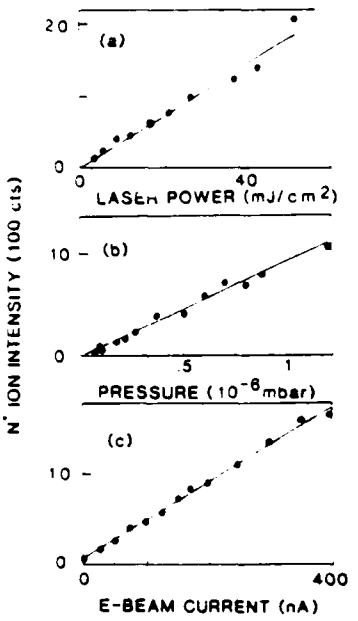

Fig. 5. Laser-enhanced N^+ ion intensities (A − B) at (a) varied laser powers, (b) N_2 gas pressures and (c) electron beam currents. The electron energy is 22.0 eV.

of 323 nA, electron energy of 22.1 eV and laser flux of 20 mJ cm^{-2}. The laser-enhanced ion intensity is linearly dependent on the gas pressure. This result again agrees with the expectation of Eq. 2.

The laser enhanced ion intensity was measured as a function of electron beam current as shown in Fig. 5c. The data were taken at an electron energy of 22.0 eV, gas pressure of 1.0×10^{-7} mbar and laser flux of 32 mJ cm^{-2}. The dependence is linear up to an electron beam current of 400 nA. This result is again consistent with Eq. 2.

The above experimental results conclusively support that the laser-enhanced N^+ ion signal is produced by dissociative electron-impact ionization of excited N_2^*, which is most likely in the $A^3\Sigma_u^+$ state. It is of interest to measure the electron excitation function of this excited species, because the data are not yet known and they are needed for many applications. The electron-impact ionization functions for N_2 in the excited and the ground states are shown in Fig. 6. The data were taken at a constant electron beam current of 217 nA, N_2 gas pressure of 7.6×10^{-8} mbar and laser flux of 40 mJ cm^{-2} each pulse. Fig. 6a is the data taken by channel A that collects the ion signals from both N_2 and N_2^*, Fig. 6b is the data of channel B that collects ion signal only from N_2, and Fig. 6c is the difference of A and B that represents the ion signal from N_2^*.

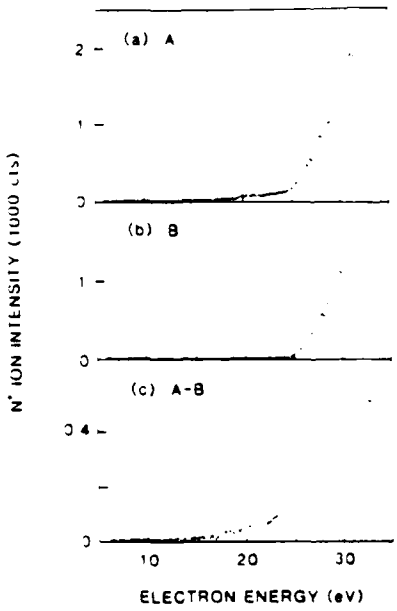

Fig. 6. Excitation function for the production of N^+ from electron impact of N_2^* and N_2. (a) Signal accumulated by channel A that includes both N_2 and N_2^*. (b) signal accumulated by channel B that includes only N_2, and (c) the difference of A and B that represents the relative dissociative ionization cross-sections of N_2^* in the range 17–24.3 eV and the difference of the dissociative ionization cross-sections of N_2^* and N_2 and the range 24.3–32 eV.

The N^+ ions shown in Fig. 6b appear at about 24 eV, which agrees with the threshold energy (24.3 eV) for the dissociative ionization of N_2 in the ground state within the electron energy resolution of 0.5 eV. The laser-enhanced N^+ ion intensities appear at a threshold of about 17 eV, as shown in Figs. 6a and 6c. The signals shown at an electron energy below 17 eV are too small to be statistically significant. The difference between the observed thresholds of N_2 and N_2^* is about equal to the laser photon energy (6.4 eV) within an experimental uncertainty of 0.7 eV. The threshold of N_2^* is not precisely determined, because the laser-enhanced signal is quite weak and the electron energy resolution is broad. Nevertheless, the observed energy thresholds do support the assertion that the laser-enhanced ion signal is produced by the excited species. The excitation function can be normalized to absolute cross-section once the value at a certain electron energy is determined.

As shown in Fig. 6c, the electron excitation function increases slowly with electron energies smaller than 25 eV and then increases rapidly with the higher energy, indicating that the N^+ ions are produced by two different processes. The slow increase channel at low electron energies may be due to

excitation to the $N_2^+(C^2\Sigma_u^+ v \geq 3)$ state which predissociates into $N^+ + N$ [22,23]. The cross-section for this process will be leveled-off at high energy. The fast increase of the excitation function is likely to be due to direct dissociative ionization channels that are available at high energy. However, the fast increase may be partly due to the high statistical uncertainty in the high electron energy region.

CONCLUDING REMARKS

N_2 was excited by ArF laser photons and then impacted by electrons. Laser-enhanced N^+ ion signals start to appear at an electron energy lower than the dissociative ionization threshold energy of N_2 by an amount about equal to the laser photon energy. The laser-enhanced signals are due to dissociative ionization of excited N_2^* in the $A^3\Sigma_u^+$ state by electron impact. The laser-enhanced N^+ ion signals depend linearly on laser flux, gas pressure and electron beam current. The excitation function for the production of N^+ from electron impact ionization of N_2^* is measured in the energy range 17–32 eV.

ACKNOWLEDGMENT

The authors wish to thank Steve Didisse at San Diego State University for the construction of the electron gun. This work is sponsored by the SDIO/IST and managed by ONR under Grant No. N00014-86-K-0558.

REFERENCES

1 D.E. Shemansky, J. Chem. Phys., 64 (1976) 565.
2 G. Cernogora, L. Hochard, M. Touzeau and C.M. Ferreira, J. Phys. B, 14 (1981) 2977.
3 B. Massabieaux, A. Plain, A. Ricard, M. Capitelli and C. Gorse, J. Phys. B, 16 (1983) 1863.
4 (a) M.M. Pejović, D.A. Bosan and S.M. Golubović, Acta Phys. Hung., 59 (1986) 273. (b) N.A. Bogatov, T.V. Borodachova, M.S. Gitlin, S.V. Goluber, I.N. Polushkin and S.V Razin, 8th Europ. Sect. Conf. Atom. Molec. Phys. Ion Gas, Greifswald, G.D.R., August 1986.
5 B.M. Jelenković and A.V. Phelps, Phys. Rev. A, 36 (1987) 5310.
6 C.J. Cook and J.R. Peterson, Phys. Rev. Lett., 9 (1962) 164.
7 D. Rapp, P. Englander-Golden and D.D. Briglia, J. Chem. Phys., 42 (1965) 4081.
8 N.R. Daly and R.E. Powell, Proc. Phys. Soc. London, 89 (1966) 273.
9 L.J. Kieffer and R.J. van Brunt, J. Chem. Phys., 46 (1967) 2728.
10 A. Crowe and W.J. McConkey, J. Phys. B, 6 (1973) 2108.
11 S. Halas and B. Adamczyk, Int. J. Mass Spectrom. Ions Phys., 10 (1973) 157.
12 R. Locht, J. Schopman, H. Wankenne and J. Momigny, Chem. Phys., 7 (1975) 393.
13 (a). K. Köllmann, Int. J. Mass Spectrom. Ion Phys., 17 (1975) 261. (b) L. Deleanu and J.A.D. Stockdale, J. Chem. Phys., 63 (1975) 3898.

14 E. Krishnakumar and S.K. Srivastava, J. Phys. B, submitted.
15 P.B. Armentrout, S.M. Tarr, A. Don and R.S. Freund, J. Chem. Phys., 75 (1981) 2786.
16 A. Lofthus and P.H. Krupenie, J. Phys. Chem. Ref. Data, 6 (1977) 113.
17 D.E. Shemansky, J. Chem. Phys., 51 (1969) 689.
18 Extrel Inc., Pittsburgh, PA 15238, U.S.A.
19 O.J. Orient and S.K. Srivastaka, J. Chem. Phys., 78 (1983) 2949.
20 E. Krishnakumar and S.K. Srivastava, J. Phys. B, 21 (1988) 1055.
21 J.W. Dreyer and D. Perner, J. Chem. Phys., 58 (1973) 1195.
22 C.A. van de Runstraat, F.J. de Heer and T.R. Govers, Chem. Phys., 3 (1974) 431.
23 J. Tellinghuisen and D.L. Albritton, Chem. Phys. Lett., 31 (1975) 91.

Low-energy electron attachment to BCl_3

Z. Lj. Petrović,[a] W. C. Wang, M. Suto, J. C. Han, and L. C. Lee
Molecular Engineering Laboratory, Department of Electrical and Computer Engineering, San Diego [redacted], San Diego, California 92182

(Received 2[redacted]1989; accepted for publication 2 October 1989)

The rate con[redacted]s of low-energy electron attachment to BCl_3 diluted in N_2 are measured as a function of E/N at 1–11 Td, corresponding to mean electron energies at 0.4–1.0 eV. The negative ions produced by hollow-cathode discharges of either pure BCl_3 or mixtures of BCl_3 in N_2 are mass analyzed to identify the products of electron attachment to BCl_3. Only Cl^- ion is found in the discharge media, although BCl_3^- is observed at the applied voltage significantly lower than the breakdown voltage. The electron attachment processes of BCl_3 are discussed.

I. INTRODUCTION

Electron attachment to electronegative gases determines the electron kinetics in gas discharges: by reducing the number and changing the energy distribution function of electrons that sustain discharges[1]; by affecting the spatial distribution of electric field and inducing double layers under certain conditions[2,3]; and by being a major source of radicals through dissociative attachment. BCl_3 is a gas of great importance for plasma technologies in microelectronics fabrication, especially for etching of aluminum.[4,5] Therefore, kinetics in discharges of BCl_3 and its mixtures were studied extensively.[5-8] However, apart from some indirect evidence, the identity of negative ions in BCl_3 discharges were not established. The swarm or beam data for electron attachment to BCl_3 are only fragmentary. Stockdale *et al.*[9] measured the thermal electron attachment rate constants of 2.7×10^{-11} cm^3/s by a drift-dwell-drift technique, and observed the excitation function of dissociative electron attachment by a beam experiment that shows a peak at 1.1 eV. On the other hand, Buchel'nikova[10] measured the cross section for the same process with an absolute peak value of 2.8×10^{-18} cm^2 at 0.4 eV. The magnitude of the electron attachment rate could be indirectly estimated from the modeling of the discharge data of Ar-BCl_3 mixtures.[7]

It is evident that the availability of the data for BCl_3 is inversely proportional to its importance. The reason for the lack of data is that BCl_3 is highly reactive and consequently difficult to handle for accurate measurements. In this paper we present the electron attachment rate constants for BCl_3 diluted in N_2. We also present the results for mass spectrometric studies of discharges of BCl_3 in N_2. The negative ions observed in discharge media provide useful information for the understanding of electron attachment processes of BCl_3.

II. EXPERIMENT

An apparatus previously used in our laboratory for electron attachment rate measurements[11] was significantly modified for this experiment. The modified apparatus shown in Fig. 1 is a stainless-steel chamber with three sections: the first section (5 in. o.d.) that is pumped by a mechanical pump is for discharge; the second section (6 in. o.d.) that is pumped by a diffusion pump (Varian, VHS-6) is for differential pumping; and the third section (4 in. o.d.), pumped by a turbomolecular pump (Varian Turbo V-450), is for the housing of a quadrupole mass analyzer (Extrel).

The apparatus operated in two modes. In mode one, the first and the second chambers were isolated, and the discharge chamber was filled to a relatively high pressure (100–400 Torr). This experiment is similar to the one described in our previous papers.[11] An excimer laser (Lumonics) was used to produce pulsed-electron swarms by irradiation of the cathode. Conduction current induced by electrons moving between electrodes was measured by the voltage drop across a resistor of 1 kΩ. The transient voltage waveforms were recorded by a digital oscilloscope (Tektronix 2430) and stored in a computer. In mode two, the first and second chambers were connected through a skimmer hole of 0.7 mm i.d. In order to keep the pressure in the mass analyzer chamber sufficiently low ($<10^{-5}$ Torr), the discharge chamber could only be filled to 1 Torr. The self-sustained dc discharge was formed between two hollow electrodes of 1 cm o.d. (Parallel plate geometry was also used for some test measurements.) The space between the two electrodes was

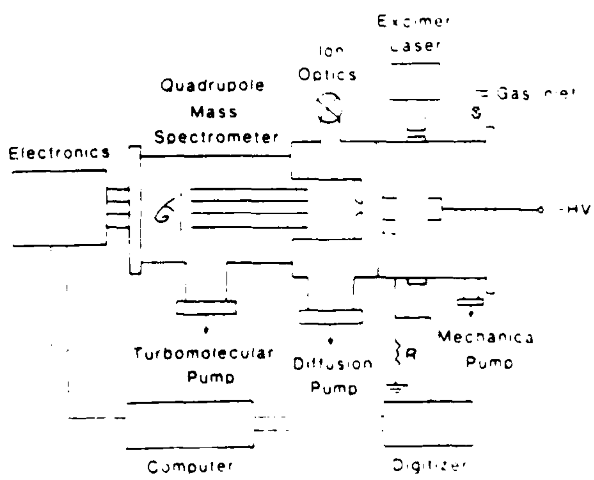

FIG. 1. Schematic diagram of the experimental apparatus.

[a] Permanent address: Institute of Physics, University of Belgrade, P.O. Box 57, 11001 Belgrade, Yugoslavia.

adjustable. Both positive and negative ions produced in discharges were sampled and mass analyzed.

For the measurement of electron attachment rates, gas mixtures of BCl_3 in N_2 were prepared in a separate stainless-steel container. The container was filled first with BCl_3, and after the container walls were saturated it was then filled with the buffer gas N_2. The volume of the connection tubing was considerably smaller than the volume of the mixing container. The initial pressure of the gas mixture was 1500 Torr, and a time of 20 h was allowed for the mixing. (Mixtures were mixed in periods between 16 and 64 h and no differences were observed.) Commercial gas mixtures were not used because the manufacturers refused to guarantee the composition of their mixtures.

Measurements were carried out in a flow system of 540 sccm for 200 Torr. At the beginning of the experiment, the pure buffer gas was allowed to flow, and the voltage waveforms induced by laser irradiation of the cathode were recorded (see Ref. 11 for the more detailed description of the experimental procedure). The BCl_3 in N_2 mixture was then added to the flow. Typically, 2–15 sccm of mixture was added that was measured and controlled by a MKS flow controller. Sufficient time was normally allowed to saturate the walls of the tubing and the chamber before the measurements commenced. Following this procedure, mixtures could be made with the abundance of BCl_3 between 0.1% and 0.5%. The experimental results were reproducible if this procedure was followed carefully. The reproducibility of the BCl_3 gas density was the major source of uncertainty. For the mass analysis of the negative ions, both pure BCl_3 and gas mixtures of about 0.5% BCl_3 in N_2 were used for discharges. The ion density was measured as a function of discharge current and gas pressure.

The BCl_3 gas was supplied by Matheson with a stated purity of 99.9% minimum. The gas sample was analyzed by the mass spectrometer in this experiment. Trace amounts of Cl_2 and $BFCl_2$ were observed in the mass spectrum, but the total impurity concentration was estimated to be smaller than 0.1%.

III. RESULTS AND DISCUSSION

A. Electron attachment rate constants

At each E/N, the electron attachment rate constants were measured at several BCl_3 concentrations for the gas mixtures of BCl_3 in N_2. The data extrapolated to the zero BCl_3 abundance are shown in Fig. 2 for the E/N in the range of 1–11 Td (1 Td = 10^{-17} V cm^2), corresponding to mean electron energy in the 0.4–1 eV range. Measurements at E/N lower than 1 Td were difficult because of low signals and the need to use more diluted mixtures which caused poor reproducibility. Nevertheless, it is evident that the trend of increase towards low E/N does not continue below the data points presented in Fig. 2. The experimental uncertainty was estimated to be within 30% of the given value. The uncertainty contains (1) geometric distribution, E/N determination, and pressure measurement, $\sim 2\%$, (2) waveform determination, $< 1\%$, (3) statistical fluctuations of the measured rates, $< 5\%$–7%, extrapolation to zero abundance, $< 5\%$–10%, and (4) uncertainty in gas mixture composition, $< 10\%$. We have set the overall uncertainty to be higher than the estimated value, because of the difficulty inherent in handling the BCl_3 gas.

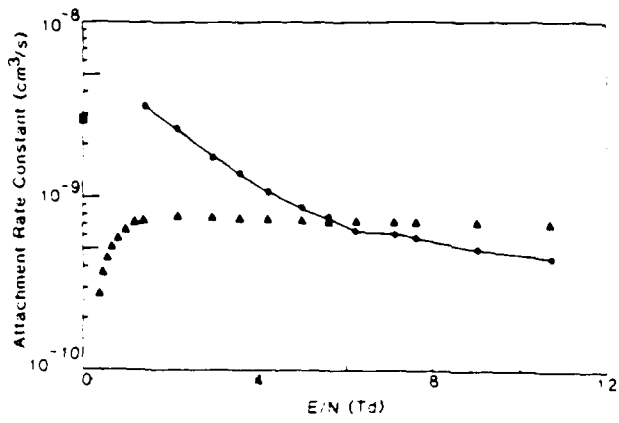

FIG. 2. Electron attachment rate constants of BCl_3 in N_2 as a function of E/N. Present data are shown as dots and are connected by lines as a guide for the eye. The results calculated from the cross section of Buchel'nikova (Ref. 10) are shown as triangles, and the thermal electron attachment rate constant of Stockdale *et al.* (Ref. 9) is shown as a rectangle.

The strong dependence of the attachment rate constant on E/N suggests that the attachment be a three-body process with a peak at low energy. As determined by thermochemical data[12] and the electron affinity[13] of Cl, the threshold for the dissociative attachment process of $e + BCl_3 \rightarrow BCl_2 + Cl^-$ is about 1.0 eV. This threshold is above the electron energy range studied in this experiment. Therefore, BCl_3^- is the only ion possibly produced at low-energy electron attachment (BCl_3^- was in fact observed in the low-pressure experiment described in the next section.) This result is consistent with the conclusion of Gottscho and Gaebe[7] who attribute BCl_3^- as the dominant negative ions observed in the RF discharge of pure BCl_3. Nevertheless, our measured attachment rate constants are not significantly dependent on gas pressures in 100–400 Torr; that is, the attachment is like a two-body process. Our observation is, in fact, consistent with the earlier observation[9] that the thermal electron attachment rate constant was not dependent on the gas pressures at 5–15 Torr. The negative ions in these measurements were not mass analyzed, because the gas pressures were very high.

We have also performed measurements for the BCl_3–Ar mixtures. Unfortunately, the results were not as reproducible as the data for N_2. The basic difficulty was that the extrapolation to zero BCl_3 abundances could not be easily performed because the measurements could not be extended to sufficiently low abundances, because the influence of the attaching gas on the electron drift velocity in Ar was large in the most interesting range. However, the crude experimental results indicate that the attachment rate constants increase in the mean electron energy range of 1.5–2.5 eV.

The electron attachment rate constants converted from the cross sections of Buchel'nikova[10] are shown in Fig. 2 for comparison. The calculation method was described in a previous paper by Petrovic and co-workers.[11] Our results agree with the calculated values in the order of magnitude, but the

E/N dependence is different. The agreement is only accidental because the attachment mechanism is quite different; that is, these results cannot be regarded as in agreement. However, our measurements at low E/N agree with the thermal electron attachment rate constant measured by Stockdale *et al.*[7] as shown in Fig. 2.

The measured attachment rate constants are too large to be affected by the possible impurities, such as Cl_2. The impurity level of Cl_2 was determined to be less than 0.1% that will contribute to the electron attachment rate constant at most 2×10^{-9} cm^3/s, in considering that the maximum rate constant of Cl_2 is only 2×10^{-7} cm^3/s at 0.06 eV.[14] The other possible impurity, $BFCl_2$, may have electron attachment rate constant similar to BCl_3 so that the small impurity level does not cause a significant effect. Some molecules such as SF_6 and CCl_4 could cause a similar attachment coefficient if they present on 1% level. We have carefully scanned the mass spectrum up to the mass number of 190, but such impurities were not detected.

B. Negative ions in discharges of BCl_3

The negative ions produced by discharges were observed for the product analysis of electron attachment to BCl_3. Initial studies of negative ions presented in discharges were carried out in a parallel plane geometry with either pure BCl_3 or its mixture with N_2. Later, most measurements were performed with hollow-cathode discharges using diluted mixtures (0.5% BCl_3 in N_2). In all cases, only Cl^- ions were found as shown in Fig. 3(a). In dc discharges, the mean electron energy may be too high to enable the production of BCl_3^-, in contrast to the bulk of rf plasmas[15] where thermal energy electrons exist for the production of BCl_3^-. When the applied voltage was lowered below breakdown voltage (for instance, 120 V) and photoelectrons were produced by irradiation of the cathode with ArF laser photons, BCl_3^- ions were observed in the gas mixture of trace BCl_3 in 0.66-Torr N_2. This observation indicates that BCl_3^- can be produced by attachment of low-energy electrons to BCl_3 and survive for a sufficiently long time such that it can be detected either by our mass analyzer or to affect the current waveform. One should, however, keep in mind that for such conditions the BCl_3^- signal would be very small (as observed by us that is about 10% of Cl^-), because the mean electron energy is so high that it favors the dissociative attachment.

The Cl^- ion intensity was measured as a function of the discharge current and the pressure. The ion intensity has a peak between 2 and 3 mA of discharge current as shown in Fig. 3(b), where the electrode space was fixed at 2 cm, the gas pressure was 0.6 Torr, and the discharge current was varied by adjusting the applied voltage (784 V at the maximum Cl^- intensity). For a fixed discharge current of 2 mA, the ion intensity had a rather sharp maximum at 400 mTorr as shown in Fig. 3(c), where the electron space was 2 cm, and the applied voltage was 784 V.

The observed Cl^- ions are produced by the electron dissociative attachment process that has a sharp peak at the energy of about 1 eV as observed by Stockdale *et al.*[7] This basic result implies that in our measurements, the mean electron energies are varied along with the changes of discharge

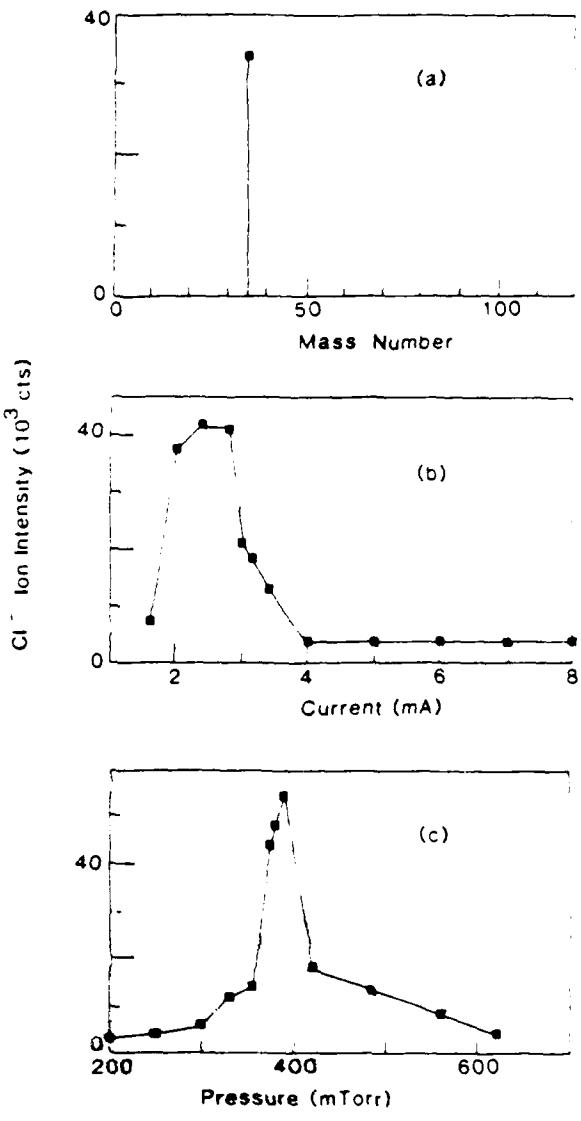

FIG. 3. Cl^- ions observed in hollow-cathode dc discharges. (a) Mass spectrum of negative ions present in the discharges of gas mixtures of 0.5% BCl_3 in N_2. (b) Dependence of the Cl^- ion intensity on the discharge current at a total pressure of 585 mTorr. (c) Dependence of the Cl^- ion intensity on the total gas pressure at a discharge current of 2 mA.

current and gas pressure, and the maximum Cl^- ion intensity corresponds to the mean electron energy in a discharge medium of about 1 eV. The phenomena could be described by the electron energy distribution function which is, however, quite complicated for the hollow-cathode discharges. In general, there are two groups of electrons[16] in a discharge medium: one group consists of the initial electrons that are accelerated in inhomogeneous but very high electric field and practically have a beamlike behavior,[17] and the second group consists of inelastically scattered and secondary electrons which have low energies. Relative magnitudes of the two groups are strongly dependent on the discharge conditions. Monte Carlo simulations[16,18,19] indicate that at these pressures the initial electrons are the dominant group. A sharp peak in the pressure dependence probably indicates the shape of the dissociative cross section, although the correspondence between the mean electron energy and the E/N

value (or the available energy for run-away electrons) in the discharge could be very nonlinear. Current dependence of the ion intensity is less sharp; but since the current-voltage dependence is not linear, it is not inconsistent with the proposed picture. However, the low ion signals at high currents may also be possibly due to the influence of space-charge force among electrons, and negative and positive ions in the bulk of discharge.

In order to establish that negative ions are originated from the discharge, but not by electron impact on BCl_3 in the transition region to the mass analyzer, we have performed the following experiment.[21] Excimer laser light was used to irradiate the region between the electrodes. As a consequence, the negative ion signal was significantly reduced. The delay between the laser light pulse and the reduction of the negative ion signal was of the order of tens of microseconds. The effect depends on the laser beam position between the electrodes. (The detailed results will be presented in a later publication.) The decrease of negative ions following laser irradiation demonstrates that the observed negative ions were produced in the discharge media, but not in the transition region, because the ion signal did not increase by the laser photoelectrons.

IV. CONCLUDING REMARKS

The electron-attachment rate constants increase toward the low E/N, indicating that the attachment is due to a three-body process. This is consistent with the observations of photodetachment thresholds that BCl_3^- is the dominant negative ion in rf discharges.[6] However, the measured attachment rate constant is not significantly dependent on the buffer gas pressure, suggesting that the attachment is apparently like a two-body process. This observation is in agreement with a previous observation[9] that the thermal electron attachment rate constant is not dependent on total gas pressure. At high pressures it is possible that the mean time between collisions is sufficiently shorter than the autodetachment time; thus, practically every excited negative ion is stabilized in the first step of attachment. At much lower pressures this might not be the case, and even more so in the low pressure region of the mass analyzer; for these cases, the BCl_3^- ions could be lost due to autodetachment. However, the BCl_3^- ion was observed by attachment of low energy electrons to BCl_3, although the BCl_3^- signal was much smaller than Cl^-.

It is worth noting that Stockdale *et al.*[9] observed a peak attachment for the two-body process of $e + BCl_3 \rightarrow BCl_2 + Cl^-$ at 1.1 eV, while at the same time they observed a relatively high thermal electron attachment rate constant. This observation is consistent with the assertion that the electron attachment is due to the three-body process at low energy, and Cl^- is produced by the two-body process at high electron energy. Our results are also consistent with this assertion that the electron attachment rate constants shown in Fig. 2 are mainly due to the three-body process, and the Cl^- ions observed in discharges are due to the two-body process.

The unpublished results of Olthoff[22] confirm the existence of BCl_3^- ions. This author has also observed that attachment for BCl_3 molecules peaks close to zero energy (both in the intensity of negative ion current and through the broadening of the zero energy peak of the electron transmission spectrum[23]). The level of impurities in his experiment is uncertain. From some theoretical considerations and the characteristics of his apparatus, the lifetime of the metastable BCl_3^- ion was estimated to be 60 μs which is consistent with our data.

ACKNOWLEDGMENTS

This paper is based on the work supported by the SDIO/IST managed by ONR under Grant No. N00014-86-K-0558, and partly by the Air Force Office of Scientific Research under Grant No. AFOSR-86-0205.

J. W. Gallagher, E. C. Beaty, J. Dutton, and L. C. Pitchford, J. Phys. Chem. Ref. Data **12**, 109 (1983); L. G. Christophorou, *Atomic and Molecular Radiation Physics* (Wiley-Interscience, London, 1971).
R. A. Gottscho, Phys. Rev. A **36**, 2233 (1987).
K. G. Emeleus, Int. J. Electron. **61**, 281 (1986); A. C. Breslin and K. G. Emeleus, Int. J. Electron. **22**, 429 (1967).
D. L. Flamm and V. M. Donnelly, Plasma Chem. Plasma Proc. **1**, 317 (1981); also, K. E. Greenberg, G. A. Hebner, and J. T. Verdeyen, Appl. Phys. Lett. **44**, 299 (1984).
R. A. Morgan, *Plasma Etching in Semiconductor Fabrication* (Elsevier, Amsterdam, 1985); T. Sugano, Ed., *Application of Plasma Process to VLSI Technology* (Wiley-Interscience, New York, 1985).
R. A. Gottscho and C. E. Gaebe, IEEE Trans. Plasma Sci. **PS-14**, 92 (1986).
G. R. Scheller, R. A. Gottscho, T. Intrator, and D. B. Graves, J. Appl. Phys. **64**, 4384 (1988); R. A. Gottscho, G. R. Scheller, D. Stoneback, and T. Intrator, J. Appl. Phys. **66**, 493 (1989).
G. R. Scheller, R. A. Gottscho, D. B. Graves, and T. Intrator, J. Appl. Phys. **64**, 598 (1988); R. A. Gottscho, G. R. Scheller, T. Intrator, and D. B. Graves, J. Vac. Sci. Technol. A **6**, 1393 (1988).
J. A. Stockdale, D. R. Nelson, F. J. Davis, and R. N. Compton, J. Chem. Phys. **56**, 3336 (1972).
I. S. Buchel'nikova, Sov. Phys. JETP **35**, 783 (1959); also, L. G. Christophorou and J. A. D. Stockdale, J. Chem. Phys. **48**, 1956 (1968).
L. C. Lee and F. Lu, J. Appl. Phys. **56**, 3169 (1984); W. C. Wang and L. C. Lee, J. Appl. Phys. **57**, 4360 (1985); Z. Lj. Petrovic, W. C. Wang, and L. C. Lee, J. Appl. Phys. **64**, 1625 (1988).
M. W. Chase, Jr., C. A. Davies, J. R. Downey, Jr., D. J. Frurip, R. A. McDonald, and A. N. Syverud, J. Phys. Chem. Ref. Data **14** Suppls. 1 and 2 (1985).
A. Christodoulides and L. G. Christophorou, *Electron Molecule Interactions and Their Applications*, edited by L. G. Christophorou (Academic, Orlando, 1984), Vol. 2.
D. L. McCorkle, A. A. Christodoulides, and L. G. Christophorou, Chem. Phys. Lett. **109**, 276 (1984).
C. A. Andersen, W. G. Graham, and M. B. Hopkins, Appl. Phys. Lett. **52**, 783 (1988).
S. Hashiguchi and M. Hasikuni, Jpn. J. Appl. Phys. **27**, 1010 (1988).
B. M. Jelenkovic and A. V. Phelps, Phys. Rev. A **36**, 5310 (1987); A. V. Phelps, B. M. Jelenkovic, and L. C. Pitchford, Phys. Rev. A **36**, 5327 (1987); A. V. Phelps and B. M. Jelenkovic, Phys. Rev. A **38**, 2975 (1988).
D. Bhasavanich and A. B. Parker, Proc. R. Soc. London A **358**, 385 (1977).
T. J. Moratz, J. Appl. Phys. **63**, 2558 (1988).
R. J. Carman, J. Phys. D **22**, 55 (1989).
J. C. Han, M. Suto, and L. C. Lee (unpublished, 1989).
J. K. Olthoff, Ph.D. thesis, University of Maryland, 1985.
J. A. Tossell, J. H. Moore, and J. K. Olthoff, Int. J. Quantum Chem. **29**, 1117 (1986).

Appendix E

TRANSIENT SIGNALS INDUCED BY LASER IRRADIATION OF NEGATIVE IONS IN HOLLOW ELECTRODE DISCHARGES OF Cl_2 AND HCl IN N_2

J. C. Han, Masako Suto and L. C. Lee
Molecular Engineering Laboratory
Department of Electrical & Computer Engineering
San Diego State University
San Diego, California 92182

and

Z. Lj. Petrovic
Institute of Physics
University of Belgrade
P.O. Box 57
11001 Belgrade, Yugoslavia

Abstract

A technique for sampling negative ions in hollow-cathode and hollow-anode discharges of strongly electronegative gases is presented. The negative ions were mass-analyzed to be Cl^-, Cl_2^- and Cl_3^- for the Cl_2/N_2 mixture and Cl^- for HCl/N_2. The dependence of negative ion intensity on gas pressure and discharge voltage was investigated. Photodetachment of negative ions was used to induce photoelectron transient signals that probe the ion concentrations. The transient signal indicates that the negative ions are original from the discharge, but not produced in the mass analyzer region by high energy electrons. Time dependence of the negative ion signal was measured by a quadrupole mass analyzer and used to study the kinetics of charged particles responsible for the transport of the laser-induced perturbation. The observed negative ion transient signal could be a useful means for studying the negative ion kinetics in plasma.

I. Introduction

The role of negative ions and electrons in the kinetics of gaseous discharges are not well understood, even though they are important in determining discharge characteristics. Discharges of electronegative gases are so often used in plasma technological applications[2] (for example, etching of electronics materials), because they can efficiently produce desirable radicals. Substitution of electrons by negative ions can lead to reduced sheath fields[3], formation of double layers[4], and significant changes in the spatial distribution of chemical species and consequently chemical reactions[5,6]. Negative ions can be the primary agents in some desirable effects such as etching[7], certain ion-molecule reactions, and modification of the I-V characteristic, while they can cause non-desirable effects such as dust formation in the silane discharges[8]. The information of negative ions in gaseous discharges could be useful for the gaseous dielectrics and switching applications[9,10]. There, photodetachment can be used to trigger fast switching modes[11], while the energy dependence of the attachment coefficient can be used to create or enhance the negative differential conductivity necessary for the operation of fast opening diffuse discharge switches[9,12].

Photodetachment spectroscopy has been used[13] for the detection of negative ions, but the results are difficult to interpret without mass analysis. Sampling of negative ions from the discharges is almost impossible because of the sheath potential which is formed to contain much mobile and energetic electrons (few eV) in the plasma, and consequently negative ions with their mean energy of the order of 100 meV cannot escape from them. In the studies of the negative ion composition of the ionosphere, special techniques that include large surface sampling plates have been used[14]. It

has been recently applied[15] to study negative ion kinetics by pulsing discharges, because electrons are dispersed much faster than the negative ions in the afterglow so that the negative ion signal can be enhanced. For an extraction of H^- ions from volume sources, magnetic field is applied to separate the plasma into two parts: one having a large density of electrons and the other dominated by negative ions that can be sampled efficiently[16]. Another technique is to operate the discharge under conditions where negative ions are the dominant charge species, and consequently the sheath fields are reduced. Sheehan and Rynn[17] showed that efficient negative ion sources can be made by reducing the electron density to below 5% of the ions density.

In this paper we present our experimental studies of the negative ion kinetics in hollow electrode discharges with and without perturbation by the excimer laser. Attempts are made to develop technique which will provide a useful means for determining both the identity and the spatial dependence of the number density of negative ions.

II. Experimental

The apparatus has been described in a previous paper[18] and is repeatedly shown in Fig. 1a. In brief, the apparatus is a stainless steel chamber with three sections: the first section (5" OD) that is pumped by a mechanical pump and a sorption pump is for the discharge, the second section (6" OD) that is pumped by a diffusion pump (Varian, VHS-6) is for differential pumping, and the third section (4" OD), pumped by a turbomolecular pump (Varian Turbo V-450), is for the housing of a quadrupole mass analyzer (Extrel).

Ions are sampled through a skimmer hole of 0.7 mm ID. In order to keep the pressure in the mass analyzer chamber sufficiently low ($< 10^{-7}$ Torr),

the discharge chamber could only be filled to 1 Torr. The self-sustained DC discharge was formed between two hollow electrodes of 1.25 cm OD as shown in Fig. 1b. The space between the two electrodes was adjustable but normally kept at 16 mm. Both positive and negative ions produced in discharges were sampled and mass analyzed.

In order to maintain the desired mixture composition, measurements were carried out in a flow system (usually 21 sccms for the buffer gas). Mixture was made by accurately controlling two flow meters, one for the buffer gas (N_2) and one for the attaching gas. Sufficient time was normally allowed to saturate the walls of the tubing and the chamber before the measurements commenced. The certified gas mixtures of 1.98% Cl_2 in He and 4.72 HCl in He were supplied by Matheson, and they were used without further purification. In each measurement, the system was filled with the gas mixture to a desired pressure, and the gas flow was maintained. Discharge was established between the two electrodes. The negative ion count was recorded as a function of gas pressure and applied voltage.

Excimer laser beam was later used to irradiate the discharge medium. As the range of an optimum condition for the production of negative ions is rather narrow, the applied voltage, pressure, and current were adjusted to obtain the maximum signal in the laser irradiation experiment. The sizes of the excimer laser beams were 20 mm x 6 mm and the laser powers were about 180 mj/pulse for the KrF laser and 150 mj/pulse for the ArF laser. Before entering the plasma region the laser beam was limited by a slit that could vary to less than 1 mm, and the laser beam in the plasma region was expanded to normally about 3 mm x 8 mm. The position of the laser beam could be moved along the axis of the discharge. Time dependence of the negative ion count was recorded following the laser pulse.

III. Results and Discussion

A. Negative Ions in Discharges

a. Cl_2/N_2 Mixture

We first present the results for the dependence of the negative ion signals on the Cl_2 pressure and the applied voltage. When a Cl_2/N_2 mixture (usually 2-4 mTorr Cl_2 in about 500 mTorr N_2) was discharged, negative ions were observed for a narrow range of experimental parameters, for which the mass spectrum is shown in Fig. 2a, where Cl^-, Cl_2^-, and Cl_3^- were observed. The Cl^- signal is much larger than those of the other two ions. The dependency of the three negative ion signals on the applied voltage for a fixed mixture of 2.8 mTorr Cl_2 in 500 mTorr N_2 are shown in Fig. 3. While all the three ions show similar voltage dependence, the Cl^- signal is always larger than the other two ions. The dependence shows a narrow feature in the 470-500 V range and a broad feature in 500-580 V. The ion signal is very sensitive to the Cl_2 pressure, thus, the data shown in Fig. 3 are only an example. The dependencies of the Cl^-, Cl_2^- and Cl_3^- ion signals on the gas pressure are shown in Fig. 4. Each ion appears in only a narrow pressure range. Cl^- and Cl_3^- have a similar pressure dependence, but Cl_2^- is quite different, indicating that they are produced by distinct processes.

b. HCl/N_2 Mixture

When HCl was used as an electronegative gas (somewhat larger percentage than that of Cl_2 was used), only Cl^- ion was detected as shown in Fig. 2b. Voltage dependence shows only one peak as shown in Fig. 5a, and the pressure dependence is also a single peak as shown in Fig. 5b. That is, the negative ions, again, only occur in narrow ranges of voltage and pressure. The general features of both Cl_2 and HCl are similar to those of BCl_3 which were presented previously[18].

c. Discussion

The general features of the dependencies of the negative ion signals on pressure and voltage are similar for all the three gas mixtures of Cl_2, HCl and BCl_3 in N_2. The negative ions occur only in narrow ranges of experimental parameters that were discussed by Petrovic *et al.*[18] and Han *et al.*[19] The reason for this phenomenon is that each negative ion is generally produced only in a narrow electron energy range which occurs only in some specific experimental conditions.

The observation that the negative ions can be sampled from discharges requires a discussion. Normally this sampling is inhibited by the anode sheath potential which is self adjusted to balance the losses of much more mobile electrons[20]. However, there are several factors which determine the magnitude of the anode fall. Most importantly, when negative ion densities are much larger than electron density or $n_-/n_e \gg \mu_e/(\mu_- + \mu_+)$, where n denotes the density and μ mobility with appropriate subscripts +, -, and e for positive ion, negative ion, and electron, then the electric field is determined by the characteristic energies of ions only[21]. In practice, this condition does not have to be strictly satisfied in order to get appreciable negative ion flux to the anode[17], but the density of electrons should be well below 5% of n_-. For chlorine containing plasmas this condition can be expected[22]. The dependence of the anode fall on current and bulk potential is complicated even without the presence of negative ions[23]. When the bulk potential is high (which is a characteristic of the discharges with electronegative gases), the anode fall is reduced[23] while the mean energy of negative ions may be increased.

Sampling of negative ions may be facilitated by the geometry of the anode and the possibility that extraction field may enter the discharge region near the sampling hole. All the above factors and the basic discharge parameters (pressure, voltage and current) basically affect the balance between the forces acting on ions due to electric filed and gas flow[24]. The relationship is complicated, and in order to take into account the possible geometric effects a two dimensional self-consistent model would be required to describe the observations reported in this paper. Having in mind the present state of the theory of gas discharges[25] such a model would be costly, and its development would require time, but it is not beyond reach. Nevertheless, the hollow anode geometry may help the sampling by creation of a strongly inhomogeneous sheath field in the region where the force field due to gas flow is maximum. Thus, the low energy ions can reach the region where the gas flow will affect their motion before being subjected to the repulsive force of the anode sheath. Though very difficult, sampling of negative ions is therefore not impossible. In the next section we will show that the negative ions collected by the mass analyzer were not produced by the impact of molecules by energetical electrons in the vacuum region behind the skimmer hole.

For a detailed understanding of the voltage and pressure dependency of the negative ion signals, apart from the above mentioned factors one should also take into account: (i) the voltage-current characteristics of the hollow electrode discharge, (ii) the energy dependence of the dissociative attachment cross section[26] convoluted with the energy distribution function for electrons which may have a non-equilibrium beam component[27], and (iii) the kinetics of negative ion formation and loss[28]. Such consideration is beyond the scope of this paper.

If the onset (or the maximum) of the negative ion peak is related to the threshold of the attachment process, then the onset[26,29] in Cl_2 would be lower than in HCl[30]. This is not observed in the experiment (Figs. 3a and 5a). In fact, the discharge voltage corresponding to the maximum of the signal is somewhat lower for HCl than for Cl_2. Therefore, it appears that in the Cl_2 and HCl discharges the mean energies and the over all electron kinetics are quite different.

Two peaks are observed in the negative ion signal versus voltage dependence for Cl_2 containing discharge (Fig. 3), and the relative magnitude of the second peak is higher for the Cl_3^- ion than the other two ions. The second peak is more probably resulted from the discharge characteristics and the balance of the sheath potential with the force due to gas dynamics rather than an indication of the second peak in the dissociative attachment cross section[26,29]. The formation kinetics of the Cl_2^- and Cl_3^- ions in a drift tube was discussed in an earlier paper by Lee *et al.*[28] Although the electron kinetics in the drift tube are quite different from those in discharge plasma, the relative abundance of the Cl_2^- and Cl_3^- ions compared to Cl^- are similar in both cases. Cl^- is produced by dissociative electron attachment to Cl_2, and Cl_3^- is likely due to the recombination of Cl^- with Cl_2, but Cl_2^- may be a result of three-body electron attachment to Cl_2. This proposed production mechanism explains that the pressure dependences of Cl^- and Cl_3^- are similar, but they are different from Cl_2^- as shown in Fig. 4.

As expected, only the Cl^- ion is observed for the discharge of HCl/N_2. The pressure and voltage dependencies of the ion signals are relatively sharply peaked, probably representing the projection of the dissociative attachment cross section into the characteristics of discharges. However, it is also possible that the mean electron energy increases at high voltage due

to input from the beam component of the hollow cathode part. Ionization then becomes more efficient, and the percentage of electrons increases thus reducing the efficiency of sampling at high voltage. (This is supported by the fact that we observe a large current increase in the voltage range covered by these measurements.) Therefore, the observed signal versus pressure/voltage dependence, which basically represents the shape of the dissociative attachment cross section convoluted by the electron energy distribution function, may not have the same proportionality for different attaching gases and discharge conditions.

B. Laser modulation of the negative ion signal

As described in the Experimental Section, KrF or ArF laser light was used to irradiate the discharge volume between the hollow electrodes (Fig. 1b). The original motivation for such experiment was to give a proof that the negative ions are not a result of electron excitation processes occurring after the skimmer hole. The fact that there is a strong modulation of the negative ion signal (up to 100%) by the laser light indicates that the negative ions indeed originate from the discharge (though some of them may be lost or converted in the mass analyzer region), but not produced after the sampling hole. Our measurements in turn gave indication that the modulation of the negative ion signal by laser pulse could be used as a diagnostic tool to identify the ion species and to measure the negative ion density.

a. Laser-Induced Transient Signals: General Features

When a discharge medium that contained a Cl_2/N_2 gas mixture was irradiated by laser pulses, the Cl^- ion signal gave a transient waveform as shown in Fig. 6a for ArF laser and Fig. 6b for KrF laser. Without the laser irradiation, the signal was in a DC level as shown by the dashed lines in Fig. 6. The general features for the transient signals are commonly observed

for different experimental conditions (discharge current, applied voltage, gas pressure, Cl_2/N_2 or HCl/N_2 mixture), although the amplitudes and the shapes of the transient signals vary with experimental parameters. The wavelength of the laser light also has a profound effect on the shape of the pulse. When ArF (193 nm) laser was used, the features of the negative ion transient signals were more pronounced than those for the KrF (248 nm) laser, especially the depth of the third peak.

Each transient signal has three distinct features: The first peak (denoted as 1 in Fig. 6a) occurs on a very short time scale (in the order of the electron transit time) following the laser pulse. It is usually largest in magnitude and always corresponds to a decrease of the negative ion signal. The second peak (2) is an increase of the signal which lasts up to a few hundred μs. The third peak (3) is greatly affected by the experimental conditions, for which the amplitude is generally larger for the ArF laser than the KrF laser.

The first peak cannot be explained as a depletion of the negative ions due to laser-induced photodetachment because it is too fast for the ionic motion to take place. We believe that this feature is related to fast moving electrons which were produced by photodetachment of negative ions. Those electrons can affect the ion signal when they reach the orifice by two possible mechanisms. One is the electron-induced collisional electron detachment, and the other is by increasing the anode sheath potential because of their high mobility. On their way to the anode the electrons get accelerated by the small electric field of the bulk and the high electric field of the hollow anode region. These energetic electrons will produce additional electrons by ionization. The secondary electrons and the initial low energy electrons can attach to Cl_2 or HCl to form Cl^- that results the second peak.

The produced negative ions drift along the field, and when the effect due to photodetached electrons is dispersed, there is an increase of ion signal in addition to the DC level that is normally detected. The fact that the second peak has a sharp increase closer to the time of the laser pulse indicates that the ionization by photodetached electrons is not homogeneous but occurs more closely to the anode when electrons gained sufficient energy. Finally, the third peak which occurs on the ion diffusion time scale represents the arrival of the negative ion density depleted by laser photodetachment. Apart from the peak value, the pulse duration gives an indication of time scale that represents important information on electron reaction kinetics and ion diffusion. A further study of this subject is of interest.

The shape of the transient signal is not affected by the possible ringing of the electrical circuit, because the noise duration generated by laser discharge system was only about 10 ns that is much shorter than the transient pulse duration (few hundred μs). The transient signal disappeared when the laser light was blocked. The magnitude of the transient signal depends on the laser intensity; thus, the signal is related to laser-plasma interaction, but not due to electrical noise. It has been demonstrated that the dynamics of the discharge current could be affected by the laser pulse, and the laser-induced pulses are often used to obtain information on the kinetics of gas discharges[31].

b. Dependencies of Transient Signals on Laser Position and Power and Discharge Voltage

The amplitudes of all three maxima increase linearly with laser power as shown in Fig. 7. Such measurements were performed in a wide range of experimental parameters, and in all cases the dependence on laser intensity was linear. This proportionality gives correlation between the transient nega-

tive ion signals and the photodetached electrons. This linearity can be in turn used to measure the density of negative ions.

The dependence of the increased Cl^- signal (the second peak) on the laser position in the plasma region is shown in Fig. 8, where the distance is measured from the cathode. For laser light close to the cathode, the effects of laser irradiation are negligible. At the middle of the discharge region there is a plateau, and then the effect suddenly increases when the laser light closes to the anode. The halfwidths of the increase Cl^- signals are also plotted as a function of laser position. The halfwidth is not critically dependent on the position as the magnitude. The position dependence is generally observed for a wide range of experimental conditions.

We have investigated the dependence of the amplitudes of the first two pulses as a function of the applied voltage in the range of voltages where we could get sufficiently good negative ion signal. The height of the first pulse changes insignificantly, while the height of the second pulse rises linearly with the voltage as shown in Fig. 9a, and the pulse duration drops with the increase of the applied voltage as shown in Fig. 9b. One should bear in mind that the current (at a fixed pressure) increases by a factor of two in the covered voltage range. When laser irradiation is fixed at the halfway between the electrodes and the chlorine abundance is changed, the height and the width of the first peak are not significantly affected, but the height of the second peak is reduced and the width increased with the increasing abundance of the attaching gas.

c. Discussion

The height of the first peak of the transient signal can be related to the density of negative ions at the point of laser irradiation. Either of the two proposed mechanisms for the ion decrease would give the proportion-

ality through it may not be linear. If electron-induced detachment causes the reduction of the negative ion signal, its reduction magnitude can be estimated from the probability that the flux of the detected negative ions (I) will be reduced by detachment by ΔI:

$$\frac{\Delta I}{I} = \frac{N_e \sigma_{ed}}{\Delta A} = \frac{(n_- I_{PH} \sigma_{PD} \Delta V)}{\Delta A} \sigma_{ed}$$

where ΔA is the cross-sectional area of the skimmer hole ($\sim 10^{-2}$ cm^2), N_e is the total number of photoelectrons, σ_{ed} is the electron-induced detachment cross section, I_{PH} is the number of laser photons per pulse per cm^2 (10^{17} cm^{-2}), σ_{PD} is the photodetachment cross section (10^{-17} cm^2), ΔV is the interaction volume of the laser and discharge (~ 0.2 cm^3). Assuming that σ_{ed} is 10^{-15} cm^2 and that n_- is 10^{13} cm^{13} cm^{-3}, one obtains $\Delta I/I \sim 20\%$. This value is in the range of experimental values.

If the decrease of negative ion signal is caused by an increase of the anode sheath due to the presence of electrons, the effects are more difficult to estimate and a full model should be developed. However, this mechanism seems to be able to easier explain 100% depletion observed in some cases.

As for the features of other two peaks, the proposed mechanism appears to be generally consistent with observations. The sudden increase of the second peak in the vicinity of the anode (Fig. 8) could possibly be explained by photoemission of electrons from the surface of the anode, but in the given picture the laser light for the last point is well far way from the anode so that the laser light may not irradiate on the anode. Also, the electrons possibly produced by laser irradiation on the anode are outside the sampling region so that the possible negative ions are not detected. We have deliberately let the laser irradiate on the anode, no signals are detected. Therefore, it is more probable that the increase is the result of the locally

reduced mean electron energy resulting in an increased attachment, and/or more negative ions near the anode that produce more photoelectrons.

IV. Concluding Remarks

The results in this paper prove possible to detect the negative ions originating from glow discharges between hollow electrodes. The negative ions present in the discharges of Cl_2 or HCl in N_2 are produced only in narrow optimum ranges of gas pressures and discharge voltages. This is caused by the reason that each negative ion is produced only in a narrow range of electron energy[18,26,29], which occurs only in a specific experimental condition.

In the second part of the paper we present the study of the transient signals caused by laser-induced photodetachment of negative ions. Three features are observed in the transient signals at the time scales of electron transit, ion drift, and ion diffusion. The first peak is a result of either electron-induced detachment or regeneration of the anode sheath by electron pulse. The other two are results of increased electron attachment and depletion of the negative ion density photodetached by the laser.

The technique presented in this paper could be used for determining the negative ion density in gas discharges. In order to accomplish this goal, further experimental studies and a detailed self-consistent theoretical description are required. This study will be extended in the future.

Acknowledgement

The authors are grateful to Dr. A. V. Phelps for some helpful comments and useful references. This papers is based on the work supported by the SDIO/IST managed by ONR under Grant No. N00014-86-K-0558.

References

1. J.W. Gallagher, E.C. Beaty, J. Dutton and L.C. Pitchford, J. Phys. Chem. Ref. Data, **12**,109 (1983); L.G. Christophorou, *"Atomic and Molecular Radiation Physics,"* (Wiley Interscience, London 1971); L.G. Christophorou, Contrib. Plasma Phys. **27**, 237 (1987).
2. R. d'Agostino, F. Cramarossa, F. Fracassi, F. Illuzzi and M.N. Armenise, J. Vac. Sci. Technol. **B 6**, 1584 (1988); D.S. Fischi and D.W. Hess, J. Vac. Sci. Technol. **B 6**, 1577 (1988); S.S. Cooperman, H.K. Choi, H.H. Sawin and D.F. Kolesar, J. Vac. Sci. Technol. **B 7**, 41 (1989).
3. J.B. Thompson, Proc. Phys. Soc. **73**, 818 (1959).
4. R.A. Gottscho, Phys. Rev., A **36**, 2233 (1987).
5. S. Radovanov, B. Tomcik, Z. Petrovic and B.M. Jelenkovic, J. Appl. Phys. (1989); B. Bletzinger and C.A. DeJoseph Jr., IEEE Trans. Plasma Sci. **PS-14**, 124 (1986).
6. Greenberg and Hargis, 89th Proc. Gaseous Electronics Conference, Palo Alto, California (1989).
7. K.J. Barlow, A. Kiermasz, W. Eccleston and J.L. Moruzzi, Appl. Phys. Lett. **53**, 57 (1988); T.R. Verhey, J.J. Rocca and P.K. Boyer, J. Appl. Phys. **63**, 2463 (1988).
8. G.S. Selwyn, J. Singh and R.S. Bennett, J.Vac. Sci. Technol **A7**, 2758 (1989); A. Garscadden in "Non Equilibrium processes in partially ionized gases," (NATO ASI series, editors, M. Capitelli and J.M. Bard).
9. L.G. Christophorou, S.R. Hunter, J.G. Carter and R.A. Mathis, Appl. Phys. Lett. **41**, 147 (1982).
10. G. Schaefer and K.H. Schoenbach IEEE Trans. Plasma Sci **PS-14**, 561 (1986), G. Schaefer, P.F. Williams, K.H. Schoenbach and J.T. Moseley

IEEE Trans. Plasma Sci. **PS-11**, 263; T. Sasagawa, A. Kawahara and M. Obara, IEEE Trans. Plasma Sci. **PS-17**, 1 (1989).

11. W.C. Wang and L.C. Lee, Trans. Plasma Sci. **PS-15**, 460 (1987); W.C. Wang and L.C. Lee, J. Phys. D **21**, 675 (1988).

12. W.H. Long Jr., W.F. Bailey and A. Garscadden, Phys. Rev. A **13**, 471 (1976); Z.Lj. Petrović, R.W. Crompton and G.N. Haddad, Aust. J. Phys. **37**, 23 (1984).

13. R.A. Gottscho and C.E. Gaebe, IEEE Trans. Plasma Sci., **PS-14**, 92 (1986); see also: P. Devynck, J. Auvray, M. Bacal, P. Belmont, J. Brutenau, R. Leroy and R.A. Stern, Rev. Sci. Instrum. **60**, 2873 (1989).

14. R.J. Cicerone and S.A. Bowhill, Radio Science **4**, 561 (1969); R.S. Narcisi, A.D. Bailey, L. Della Lucca, C. Sherman and D.M. Thomas, J. Athmos. Terr. Phys. **33**, 1147 (1971); A.A. Viggiano and F. Arnold, Planet Space Sci. **29**, 895 (1981).

15. L.J. Overzet, J.H. Beberman and J.T. Verdeyen, J. Appl. Phys. **66**, 1622 (1989).

16. M.Bacal, J.Brutenau, P.Devynck, Rev. Sci. Instrum. **59**, 2151 (1988).

17. D.P. Sheehan and N. Rynn, Rev. Sci. Instrum. **59**, 1369 (1988).

18. Z.Lj. Petrović, W.C. Wang, J.C. Han, M. Suto and L.C. Lee, J. Appl. Phys. in press (1990).

19. L.C. Lee, J.C. Han and M. Suto, Proc. Sixth International Swarm Seminar (Glen Cove 1989), p11.

20. B. Chapman, "Glow Discharge Processes" (Wiley Interscience, New York 1980).

21. G.L. Rogoff, J. Phys. D **18**, 1533 (1985).

22. G.L. Rogoff, J.M. Kramer and R.B. Piejak, IEEE Trans. Plasma Sci. **PS-14**, 103 (1986).

23. V.A. Shveigert, Sov. J. Plasma Phys. **14**, 801 (1988).

24. G.N. [illegible] and B.E. Evans, Proc. Tenth Symposium (International) on Combustion II-7-12; R.B. Tombers and L.M. Chanin, J. Appl. Phys. **43**, 2465 (1972); H.Helm, Beitr. Plasmaphys. **18**, 147 (1978).

25. J.P. Boeuf, Phys. Rev. A **36**, 2782 (1987); D.B. Graves and K.F. Jensen, IEEE Trans. Plasma Sci. **PS-14**, 78 (1986); A.D. Richards, B.E. Thompson and H.H. Sawin Appl. Phys. Lett. **50**, 492 (1987); M.S. Barnes, T.J. Colter and M.E. Elta, J.Appl. Phys. **61**, 81 (1987); V.V. Boiko, Yu. A. Mankevich, A.T. Rakhimov, N.V. Suetin, V.A. Feoktistov and S.S. Filipov, Sov. J. Plasma Phys. **15**, 126 (1989).

26. M.V. Kurepa and D.S. Belic, J. Phys. B **11** 3719 (1978).

27. S. Hashiguchi and M. Hasikuni, Jpn. J. Appl. Phys. **26**, 271 (1987); *ibid.* **27**, 1010 (1988); *ibid.* **27**, 2007 (1988); *ibid* **28**, 699 (1989).

28. L.C.Lee, G.P. Smith, J.T. Moseley, P.C.Cosby and J.A.Guest, J. Chem. Phys. **70**, 3237 (1979); M.S. Huq, D. Scott, N.R. White, R.L. Champion and L.D. Doverspike, J.Chem. Phys. **80**, 3651 (1984).

29. D.L. McCorkle, A.A. Christodoulides and L.G. Christophorou, Chem. Phys. Lett. **109**, 276 (1984).

30. Z.Lj. Petrović, W.C. Wang, and L.C. Lee, J. Appl. Phys. **64**, 1625 (1988).

31. A. Mitchell, G.R. Scheller, R.A. Gottscho and D.B. Graves, Phys. Rev. A **40**, 5199; H. Debontride, J. Derouard, P. Edel, R. Romestain, N. Sadeghi and J.P. Boeuf, Phys. Rev. **40**, 5208 (1989); G.S. Selwyn, B.D. Ai and J. Singh, Appl. Phys. Lett **52**, 1953 (1988); S.W. Downey, A. Mitchell and R.A. Gottscho, J. Appl. Phys. **63**, 5280 (1988).

Figure Captions

Fig. 1. (a) Schematic diagram of the experimental apparatus. (b) Geometrical dimensions of the electrodes and the laser beam.

Fig. 2. (a) Mass spectrum for negative ions the discharge of the Cl_2/N_2 mixture. (b) same but for HCl attaching gas.

Fig. 3. Dependence of the observed negative ion signal on the discharge voltage for (a) Cl^-, (b) Cl_2^-, and (c) Cl_3^- ions. The gas pressures were 2.8 mTorr Cl_2 in 494 mTorr N_2.

Fig. 4. Dependence of the observed negative ion signal on the gas pressure for (a) Cl^-, (b) Cl_3^-, and (c) Cl_2^- ions. The Cl_2 pressure was fixed at 2.8 mTorr, but N_2 varied. The applied voltage was fixed at 483 V. At 550 mTorr, the discharge current was about 3 mA.

Fig. 5. Dependence of the measured Cl^- signal from the discharge of the HCl/N_2 mixture as a function of (a) applied voltage ([HCl] = 11 mTorr and $[N_2]$ = 712 mTorr) and (b) gas pressure (V = 440 V; [HCl] = 11 mTorr).

Fig. 6. The general shapes of the negative ion transient signals produced from photodetachment of Cl^- by (a) ArF and (b) KrF laser photons. There are three distinct features: (1) a depletion on electron transit time scale, (2) an increase on ion drift time scale, and (3) a depletion on ion diffusion time scale. The applied voltage was 580 V. For ArF laser, the gas pressures were 3.3 mTorr Cl_2 in 717 mTorr N_2, the gap between the electrodes was 1.8 cm, and the discharge current was 3 mA. For KrF laser, the gas pressures were 3.3 mTorr Cl_2 in 817 mTorr N_2, the gap between the electrodes was 1.4 mm, and the discharge current was 2 mA.

Fig. 7. The dependence of the heights of the the three features in the transient signals on the ArF laser power. The 1, 2, and 3 represent the three peaks as shown in Fig. 6a. The data were taken under an experimental condition similar to those in Fig. 6a.

Fig. 8. The maximum value (circle) and the halfwidth (triangle) of the second peak in the transient signal of Cl^- as a function of the ArF laser irradiation position between the electrodes. The distance was measured from the cathode. It is believed that there is a proportionality between the signal and the negative ion density at the point of laser irradiation. The experimental conditions were essentially similar to those in Fig. 6 for the ArF laser.

Fig. 9. (a) Cl^- ion signals (second peak) increased by ArF laser irradiation of discharge media of Cl_2 in N_2 as a function of the applied discharge voltage. (b) The width of the increased Cl^- signal as a function of the applied voltage. The experimental conditions were same as those in Fig. 6 for the ArF laser, except for that the gas pressure was 787 mTorr. The current increased from 2 to 4.3 mA when the voltage changed from 559 to 600 V. The data were repeatedly taken at different times, for which the data taken in a short period were plotted with a same symbol.

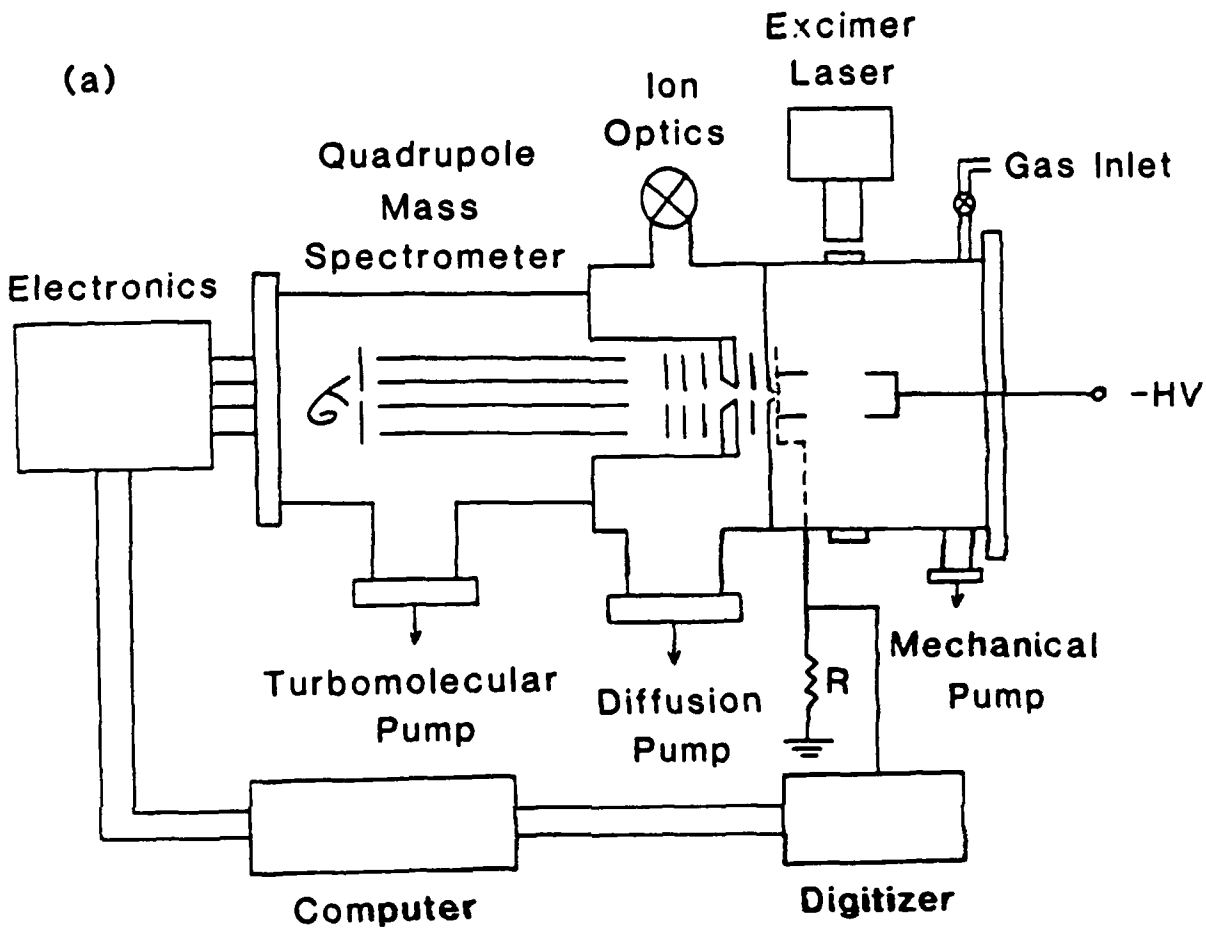
(a)
Excimer
Laser
Ion
Optics
Quadrupole
Mass
Spectrometer
Gas Inlet
Electronics
-HV
Turbomolecular
Pump
Diffusion
Pump
R
Mechanical
Pump
Computer
Digitizer

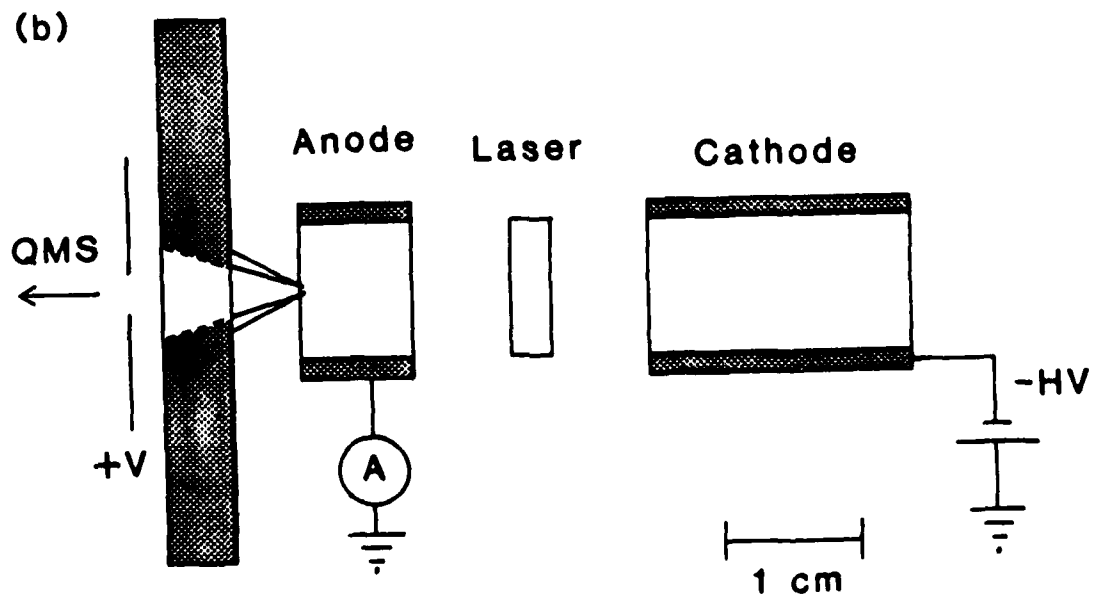
(b)
Anode
Laser
Cathode
QMS
-HV
+V
A
1 cm

Fig. 1

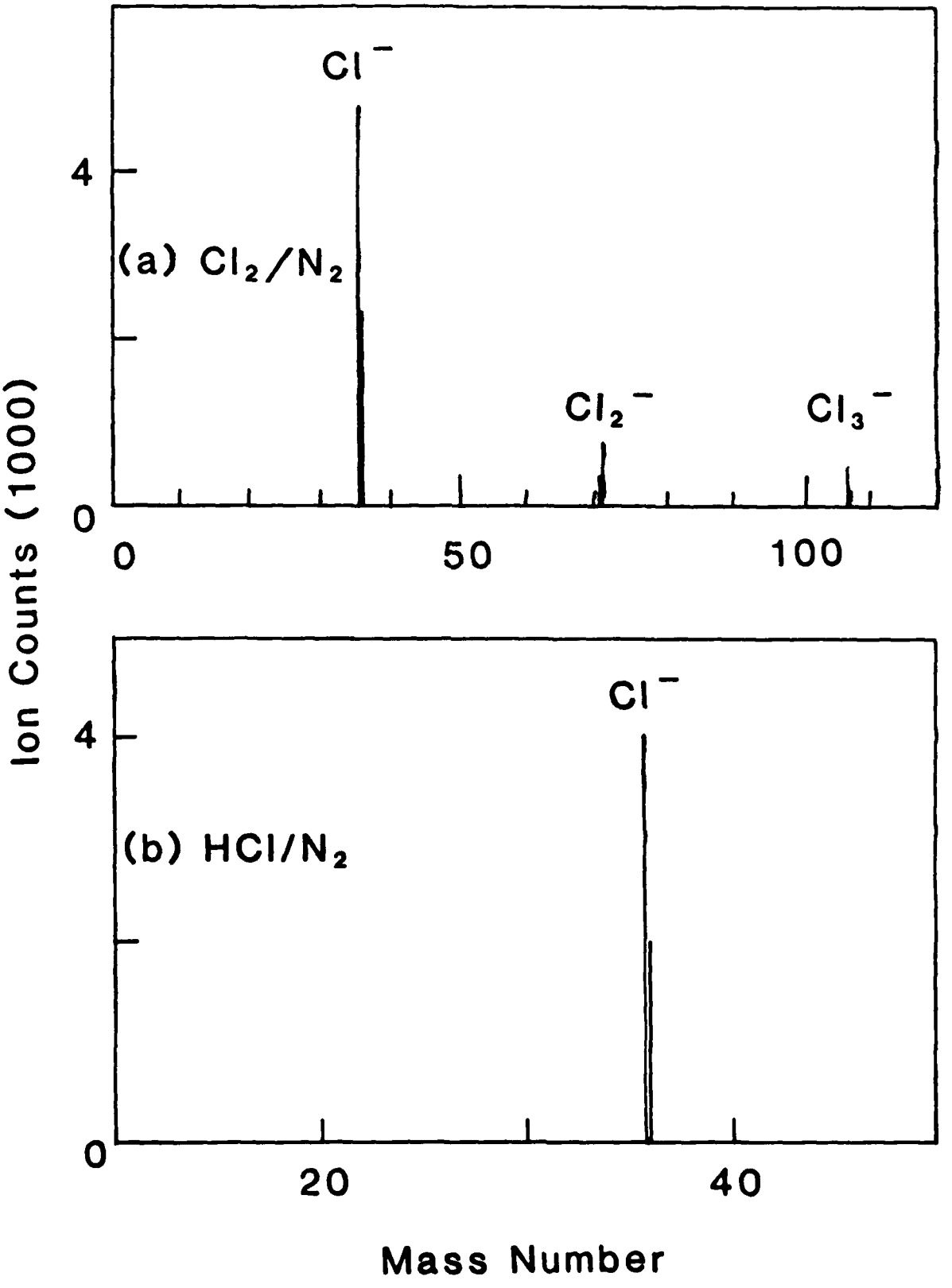
Cl⁻
4
(a) Cl₂/N₂
Cl₂⁻
Cl₃⁻
0
0
50
100
Ion Counts (1000)
Cl⁻
4
(b) HCl/N₂
0
20
40
Mass Number

Fig. 2

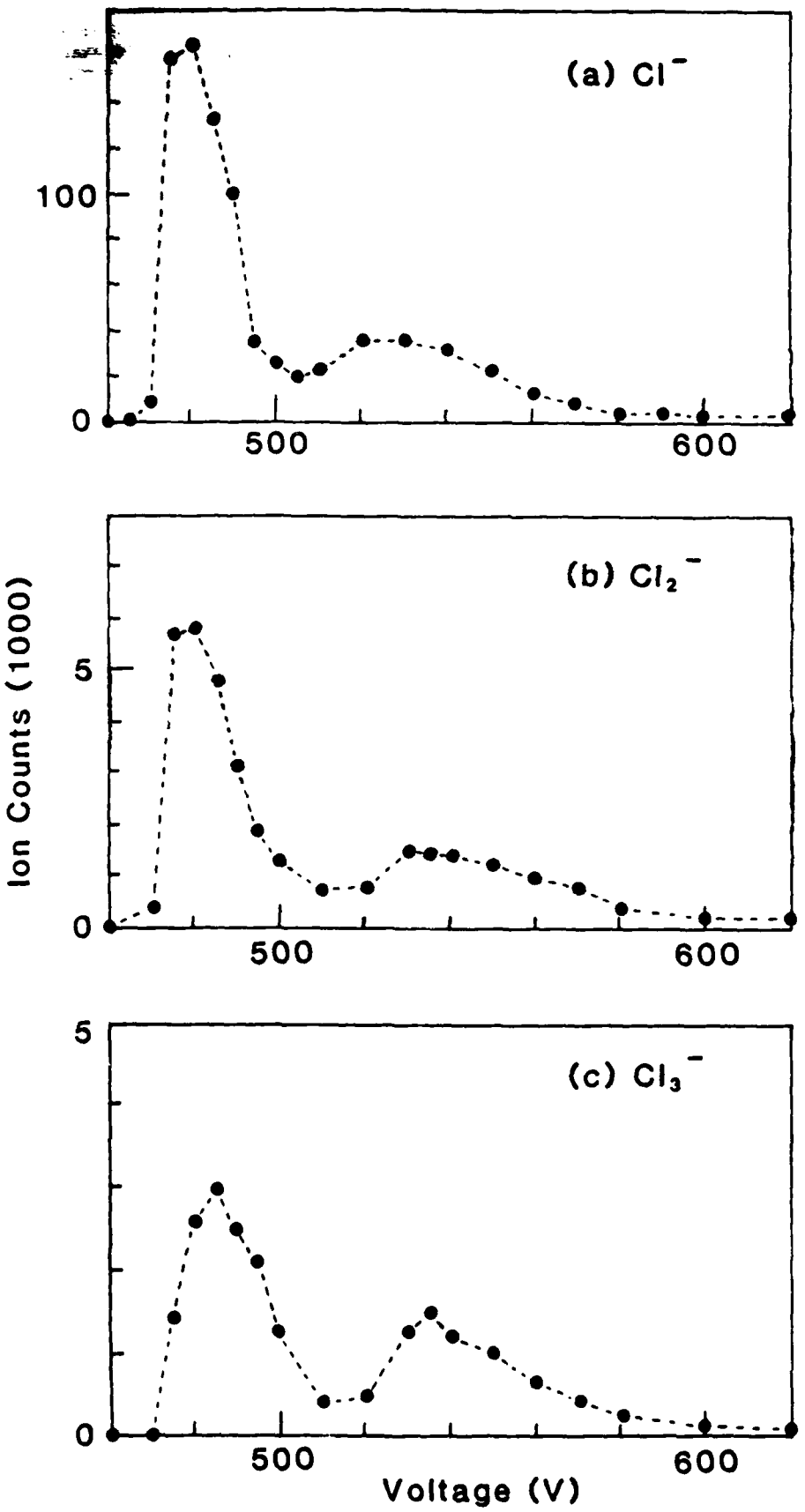
(a) Cl^-
100
0
500
600
(b) Cl_2^-
5
0
500
600
Ion Counts (1000)
5
(c) Cl_3^-
0
500
600
Voltage (V)

Fig. 3

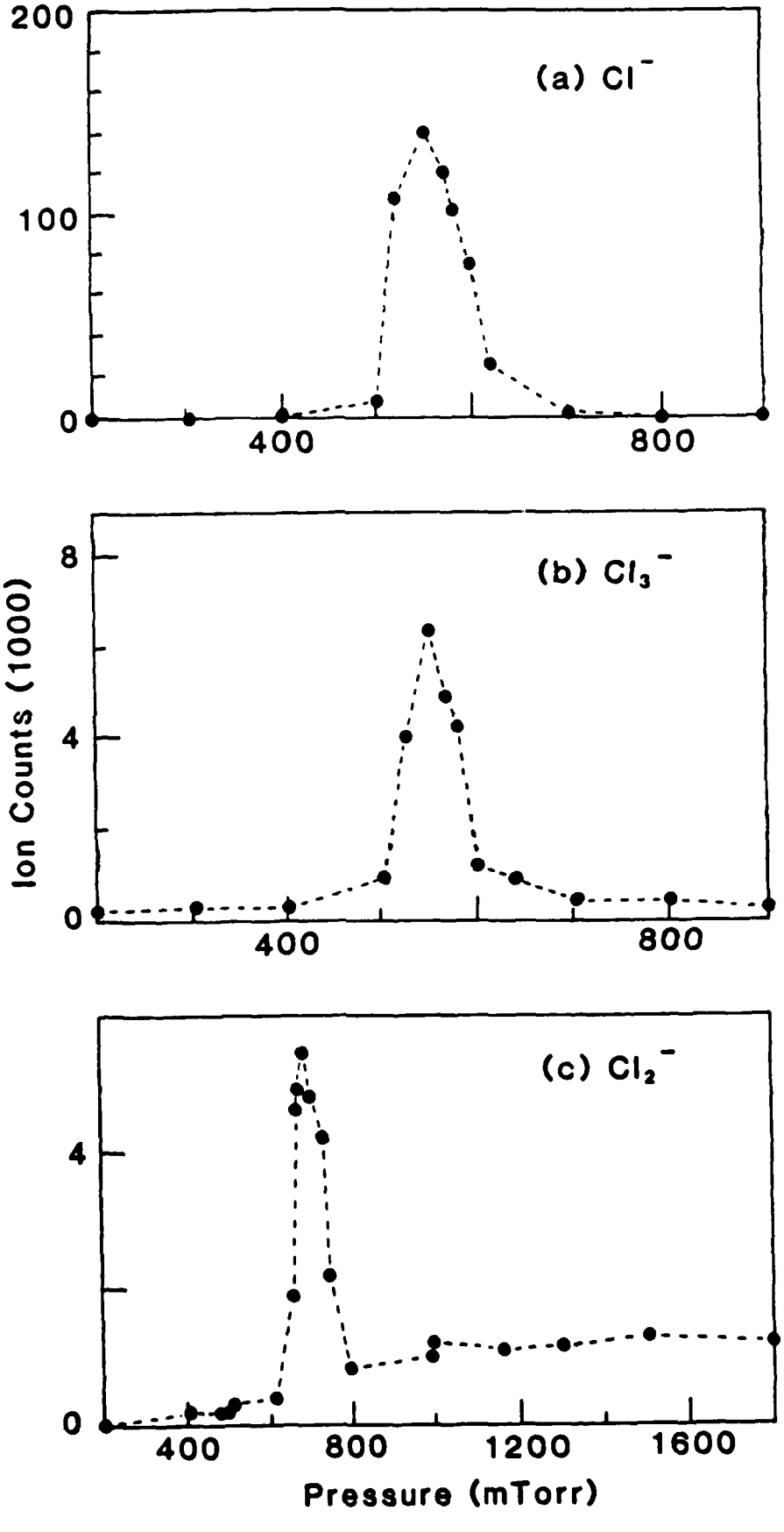
200
100
0
(a) Cl⁻
400
800
8
4
0
(b) Cl₃⁻
400
800
Ion Counts (1000)
4
0
(c) Cl₂⁻
400
800
1200
1600
Pressure (mTorr)

Fig. 4

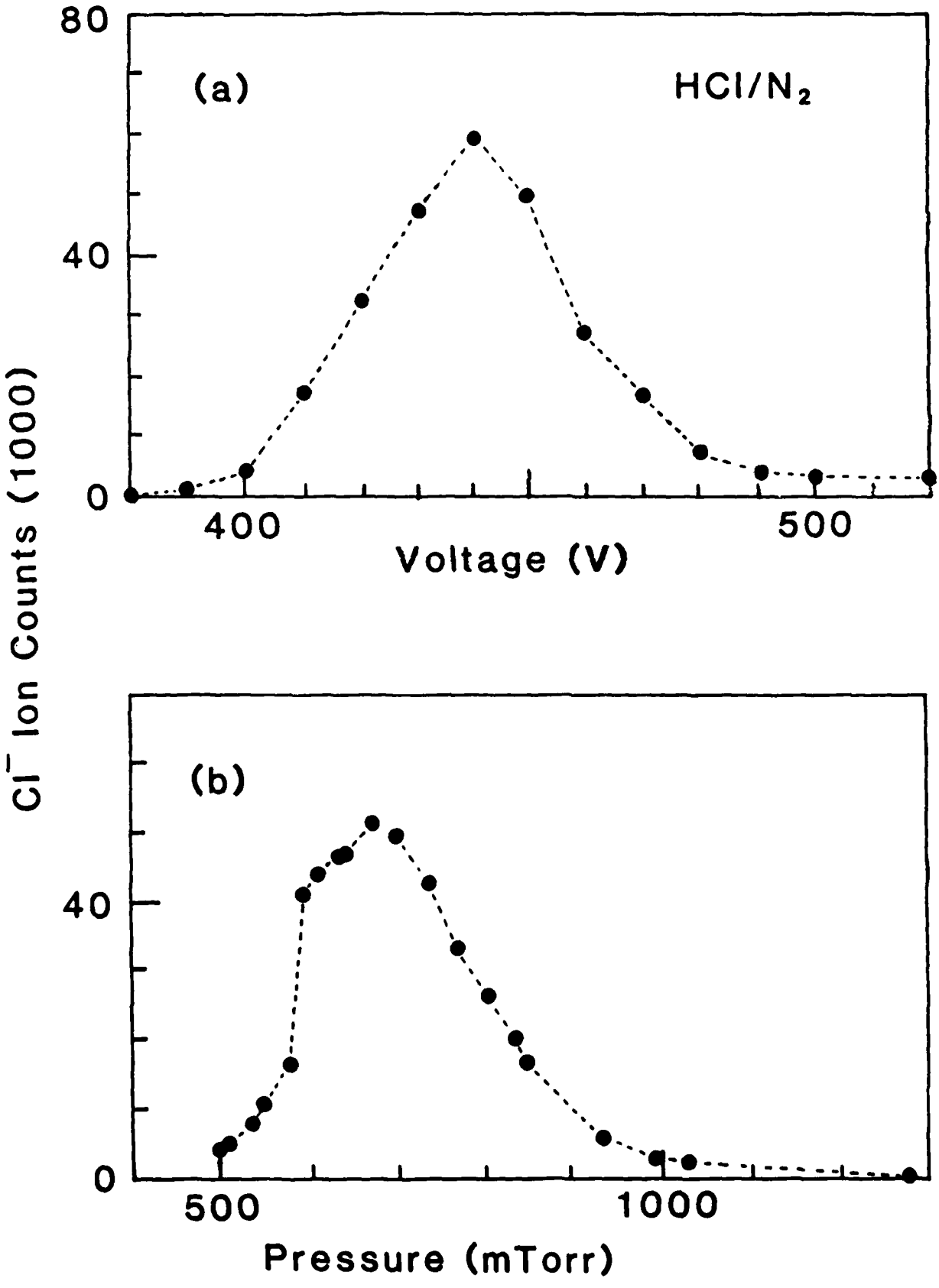
80
40
0
(a)
HCl/N2
400
500
Voltage (V)
Cl⁻ Ion Counts (1000)
(b)
40
0
500
1000
Pressure (mTorr)

Fig. 5

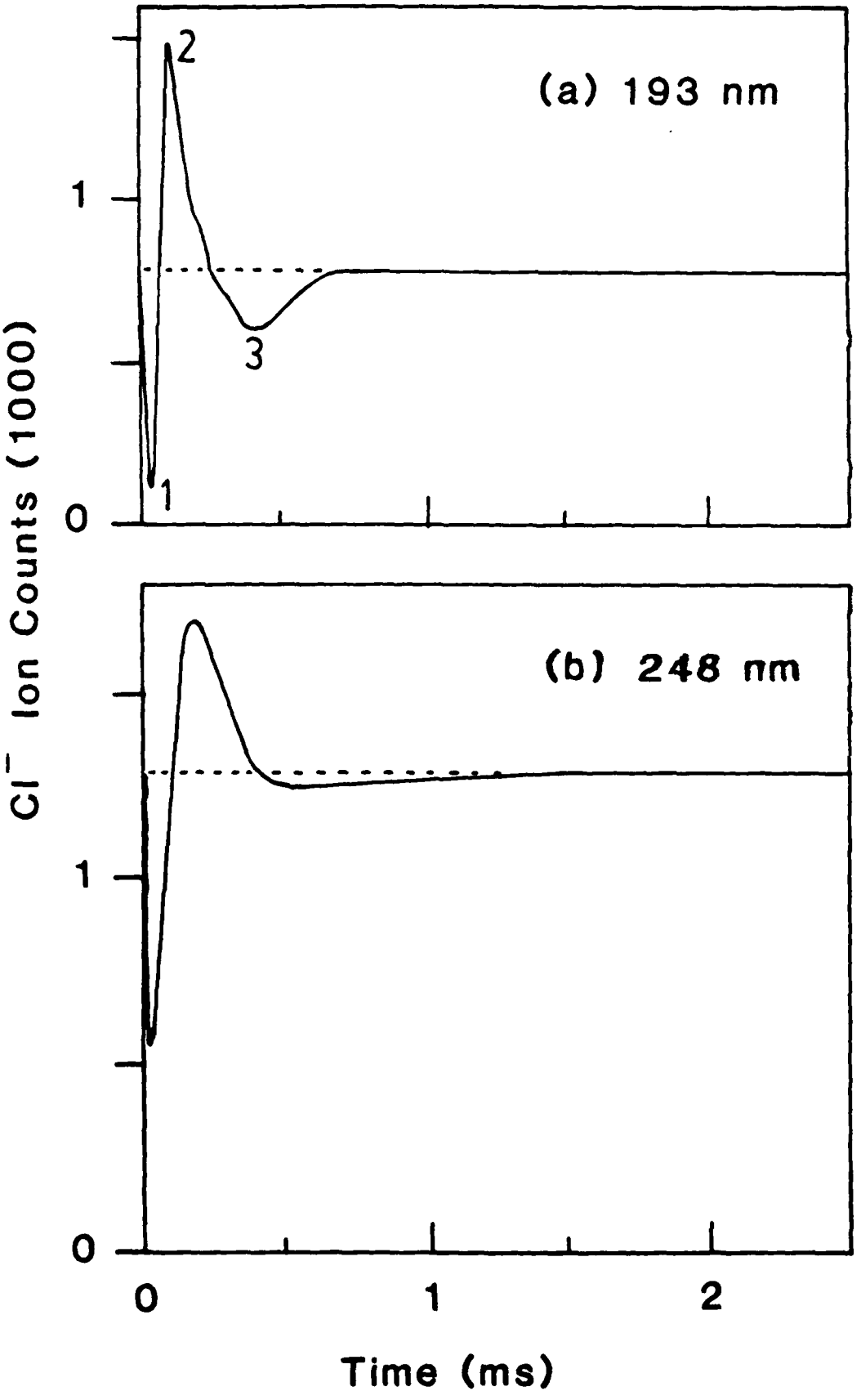

Fig. 6

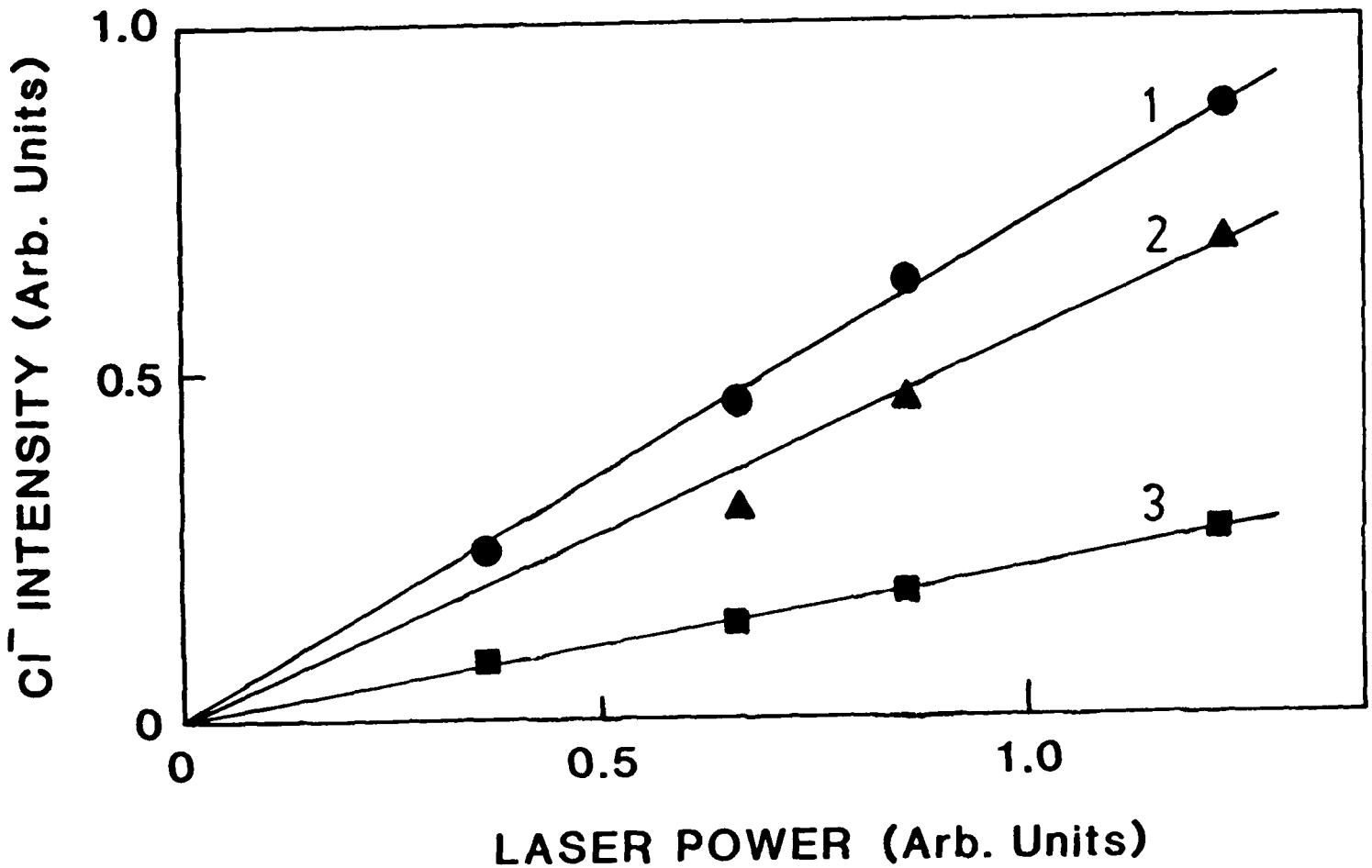
1.0
0.5
0
0
0.5
1.0
Cl⁻ INTENSITY (Arb. Units)
LASER POWER (Arb. Units)
1
2
3

FIG. 7

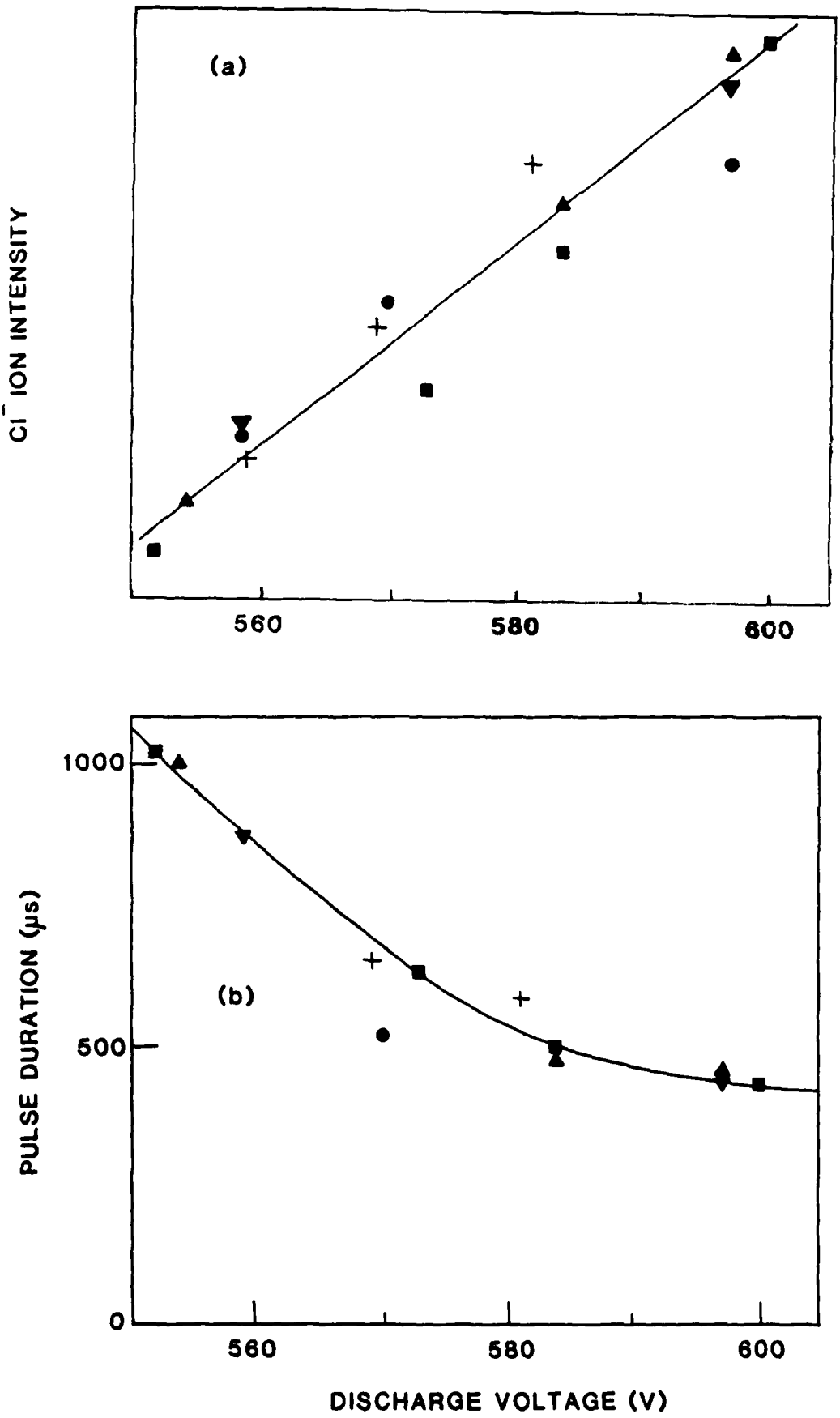
(a)
Cl^- ION INTENSITY
560
580
600
(b)
PULSE DURATION (μs)
1000
500
0
560
580
600
DISCHARGE VOLTAGE (V)

Fig. 9

Fig 8

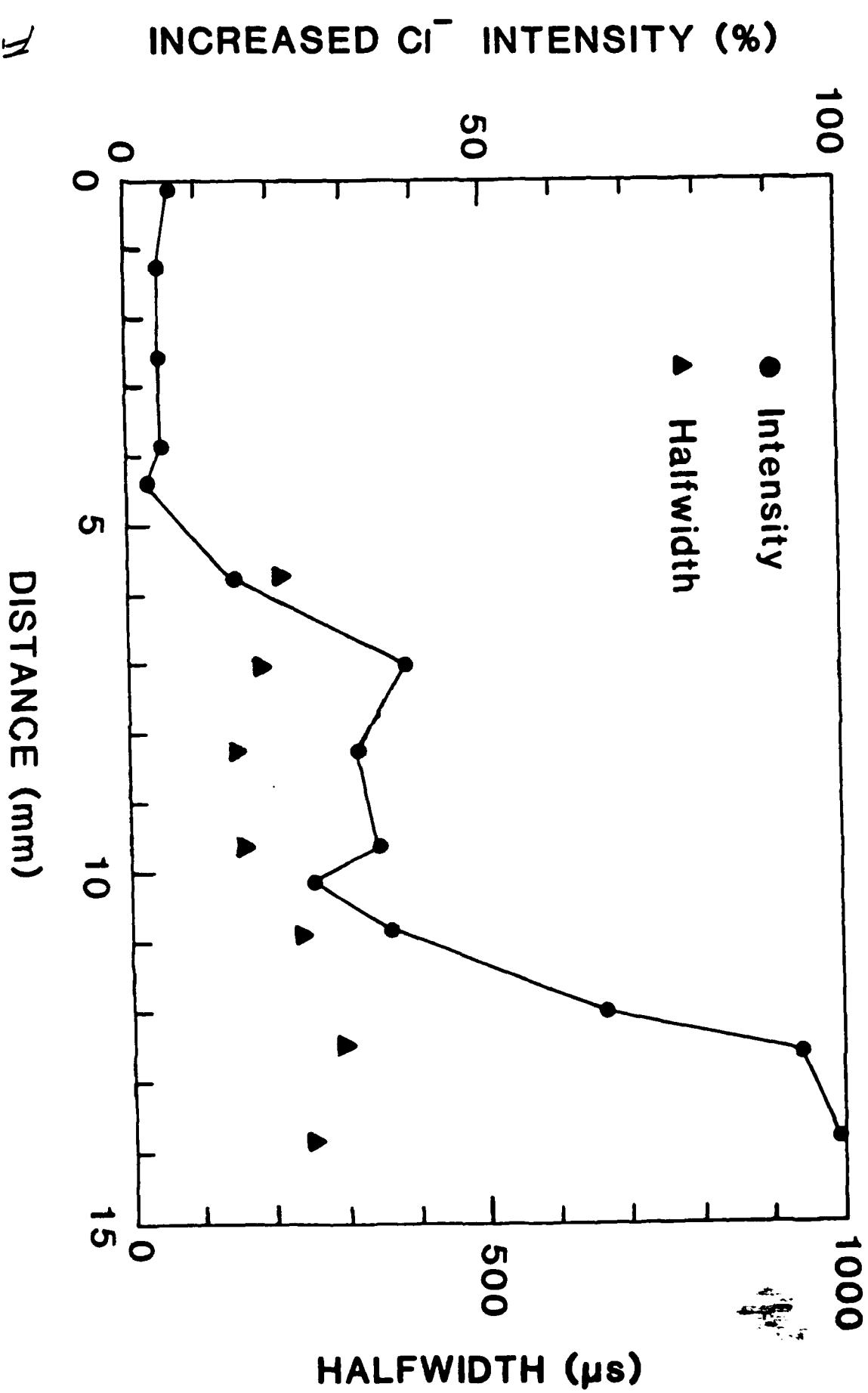
INCREASED Cl⁻ INTENSITY (%)
0
50
100
Intensity
Halfwidth
DISTANCE (mm)
0
5
10
15
0
500
1000
HALFWIDTH (μs)